arXiv:1210.8342v1 [quant-ph] 31 Oct 2012

# Theory of quantum frequency conversion and parametric down-conversion in the high gain regime

**Andreas Christ[1], Benjamin Brecht[1], Wolfgang Mauerer[2,3], and Christine Silberhorn[1,2]**

[1]Applied Physics, University of Paderborn, Warburger Straße 100, 33098 Paderborn, Germany
[2]Max Planck Institute for the Science of Light,
Günther-Scharowsky Straße 1/Building 24, 91058 Erlangen, Germany
[3]Siemens AG, Corporate Research and Technologies,
Wladimirstrasse 3, 91058 Erlangen, Germany

E-mail: `andreas.christ@uni-paderborn.de`

**Abstract.** Frequency conversion (FC) and parametric down-conversion (PDC) are among the most widely used nonlinear processes for the implementation of quantum optical experiments. Parametric down-conversion enables the efficient creation of quantum states ranging from photon-number states over squeezers to EPR-states. Frequency conversion gives rise to technologies enabling efficient atom-photon coupling, ultrafast pulse gates and enhanced detection schemes. However, despite their widespread deployment, their theoretical treatment remains challenging. Especially the multi-photon components in the high gain regime, as well as the explicit time-dependence of the involved Hamiltonians hamper an efficient theoretical description of these nonlinear optical processes.

In this paper we investigate these effects and put forward two models which enable a full description of FC and PDC in the high gain regime. We present a rigorous numerical model relying on the solution of coupled integro-differential equations which covers the complete dynamics of the process. And, as an alternative, we develop a simplified model that, at the expense of neglecting time-ordering effects, enables an analytical solution which approximates the correct solution with high fidelity in a broad parameter range.

The developed fundamental understanding of frequency conversion and parametric down-conversion gives valuable insights into the quantum properties of the processes, extends the current theoretical descriptions, and simplifies considerably the engineering process for future quantum information applications using FC and PDC.

## 1. Introduction

A fundamental building block of quantum information and quantum communication applications are nonlinear optical processes. In experimental implementations of photonic quantum systems parametric down-conversion (PDC) and frequency conversion (FC) are omnipresent. Parametric down-conversion enables the generation of various quantum states ranging from single photons [1, 2, 3, 4, 5] over entangled photon-pairs [6, 7, 8] up to squeezers [9, 10] and EPR-states [11, 12]. Frequency conversion is applied for frequency translations between different wavelengths [13, 14, 15] which enables interfaces between quantum systems, in particular atom-photon coupling [16, 17], quantum pulse gates [18, 19, 20], and efficient quantum state detection [21, 22, 23, 24, 25].

Their deployment in quantum enhanced applications requires a detailed theoretical understanding of the corresponding nonlinear interactions. A variety of models have been developed for PDC [26, 27, 28, 29, 12, 30] and FC [18, 19, 20, 15, 31]. They vary from straightforward perturbation approaches to much more rigorous treatments. The crucial issue in these derivations is firstly the fact that multi-photon effects have to be considered during the interaction, and secondly the problem that the involved electric field operators and consequently Hamiltonians do *not* commute in time. In this paper we address these issues and build two theoretical models for FC and PDC: a rigorous numerical model based on the theoretical framework of Mikhail I. Kolobov [32], and a simplified analytical approach. Both models take into account higher-order photon number effects and are hence suitable to describe FC and PDC in the high gain regime. We analyse their performance and the quality of their predictions over a broad parameter range which enables us to suggest when a simple analytic modelling of the processes is sufficient and when the rigorous approach has to be applied.

The paper is structured into two main parts: In sections 2 to 9 we study frequency conversion. Our investigation of this process is divided into eight sub chapters: After a short description of the basic principles of frequency conversion in section 2, section 3 discusses the Hamiltonian of the process. The general properties of the conversion are outlined in section 4. In section 5 we introduce the no time-ordering approximation which forms the basis for the analytical solution of the frequency conversion process and elaborate on its implications. In section 6 we derive the analytic solution excluding time-ordering effects. In section 7 we put forward the rigorous approach relying on the solution of coupled integro-differential equations. The differences between the two models are quantified in section 8. Finally, in section 9, we elaborate on the impacts of our work on the design and performance of frequency conversion processes for quantum enhanced applications. The same reasoning is then applied to the process of parametric down-conversion in sections 10 onward. Section 18 concludes the paper and summarizes our findings. Appendix A to Appendix F contain additional information and further calculations.

## 2. FC: Overview

A general frequency conversion process is sketched in figure 1. Mediated by the nonlinearity of the crystal and a strong pump beam two input fields $\hat{a}^{(in)}$ and $\hat{c}^{(in)}$ are interconverted into two output fields $\hat{a}^{(out)}$ and $\hat{c}^{(out)}$. This frequency conversion process is more commonly known as sum frequency generation (SFG), when the input beam in combination with the pump beam generates an output field at a higher frequency $\omega_{out} = \omega_{in} + \omega_p$, or difference frequency generation (DFG), when a field with frequency $\omega_{out} = \omega_{in} - \omega_p$ is created.‡

The distinction between sum-frequency and difference frequency generation arises via the input wave which is fed in either the $\hat{a}^{(in)}$ or $\hat{c}^{(in)}$ port. In the scope of this paper $\hat{a}^{(in)} \rightarrow \hat{c}^{(out)}$ depicts a sum-frequency generation process and $\hat{c}^{(in)} \rightarrow \hat{a}^{(out)}$ labels difference frequency generation. Each crystal configuration always supports both processes simultaneously and we refer to the overall system as frequency conversion.

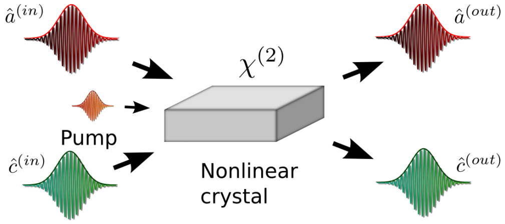

**Figure 1.** Sketch of the frequency conversion process. Mediated by the strong pump field and the $\chi^{(2)}$-nonlinearity of the medium parts of the fields $\hat{a}^{(in)}$ and $\hat{c}^{in}$ are interconverted into the two output fields $\hat{a}^{(out)}$ and $\hat{c}^{(out)}$.

In this paper we go beyond the standard monochromatic single-mode description of frequency conversion and consider a multitude of frequencies interacting with each other during the frequency conversion process. This becomes especially important for pulsed frequency conversion experiments where wave packets, spanning several nanometers in width, interact with each other. In the following chapters we derive the properties of this transformation and compare the accuracy of different theoretical models.

## 3. FC: Hamiltonian

We first define the electric field operators of an optical wave inside a nonlinear medium as [33]

$$\begin{aligned}\hat{E}^{(+)}(z,t) &= \hat{E}^{(-)\dagger}(z,t)\\ &= \imath\left(\frac{\hbar\, c}{4\pi\epsilon_0 A\, n^3(k_0)}\right)^{\frac{1}{2}} \int \mathrm{d}k\, \sqrt{\omega(k)}\, \exp\left[\imath(kz-\omega(k)t)\right] \hat{a}(k),\end{aligned} \tag{1}$$

where $A$ labels the transverse quantization area in the material [34]. We use the slowly varying envelope approximation, i.e. the bandwidth $\Delta\omega$ of the considered electric fields is small compared to their central frequency $\omega_0$ ($\Delta\omega \ll \omega_0$) and hence treat the dispersion term in front of the integral $n(k_0)$ in (1) as a constant, using the value at the central wave vector $k_0$. This approximation is justified since, in the remainder of this paper, we only consider electric fields not too broad in frequency, compared to their central frequency, and take into account the rather flat dispersion in nonlinear crystals. Finally $\hat{a}(k)$ is the standard single-photon annihilation operator which destroys a single-photon in mode $k$ and obeys

---

‡ In classical nonlinear optics, DFG is understood as a stimulated process. The bright pump field has the highest frequency and the process is seeded with a weak input field, which is enhanced through continuous conversion of pump photons. We, in contrast, assume a weak input field, which has the highest frequency and the 'seed' is the bright pump field (see [18] for details).

$$\left[\hat{a}(k), \hat{a}(k')^\dagger\right] = \delta(k - k') \qquad [\hat{a}(k), \hat{a}(k')] = 0. \tag{2}$$

In this paper we restrict ourselves to electric fields in one dimension, this means we assume a fully collinear propagation of the interacting fields along one axis in a single-spatial mode, since a three dimensional treatment does not offer further physical insight into the properties of the process and clutters the calculations.

The Hamiltonian of the frequency conversion process consists of two parts: The Hamiltonian $H_0^{(x)}$ describing the free propagation of the electromagnetic waves through the medium for each of the involved fields [32]

$$\hat{H}_0^{(x)}(t) = \frac{2\epsilon_0 A\, n_{k_0^x}^3}{c} \int \mathrm{d}z\, \hat{E}_x^{(-)}(z,t)\hat{E}_x^{(+)}(z,t), \tag{3}$$

where the factor in front of the Hamiltonian appears due to the normalization of the electric fields operators in (1) [32]. The interaction Hamiltonian of the frequency conversion process is given by [35, 36, 18, 19]

$$\hat{H}_I^{(FC)}(t) = \epsilon_0 \int \mathrm{d}z\, \chi^{(2)}(z)\, \hat{E}_p^{(+)}(z,t)\hat{E}_a^{(+)}(z,t)\hat{E}_c^{(-)}(z,t) + h.c.. \tag{4}$$

$\hat{E}_p^{(+)}(z,t)$ labels the pump field driving the frequency conversion process and $\hat{E}_a^{(+)}(z,t), \hat{E}_c^{(-)}(z,t)$ are the two fields which are interconverted. In the derivation of this Hamiltonian we used the rotating wave approximation and hence only regard the frequency conversion terms of the nonlinear optical process while neglecting the parametric down-conversion and further nonlinear interactions. The pump field driving the frequency conversion process is a strong optical wave. We hence treat it as a classical field:

$$E_p^{(+)}(z,t) = E_p^{(-)*}(z,t) = \mathcal{A}_p \int \mathrm{d}k\, \alpha\left[\omega(k)\right] \exp\left[\imath(kz - \omega(k)t)\right] \tag{5}$$

Here $\mathcal{A}_p$ labels the pump amplitude and $\alpha\left[\omega(k)\right]$ its spectral distribution ranging from $\delta(\omega - \omega_c)$ for cw-laser sources up to more complicated forms in the case of pulsed laser systems. We further assume that the pump field is not depleted during propagation through the crystal since only a minor part of the strong pump beam is lost during the frequency conversion process. The interaction Hamiltonian (4) becomes:

$$\hat{H}_I^{(FC)}(t) = \epsilon_0 \int \mathrm{d}z\, \chi^{(2)}(z)\, E_p^{(+)}(z,t)\hat{E}_a^{(+)}(z,t)\hat{E}_c^{(-)}(z,t) + h.c.. \tag{6}$$

Combining (3) and (6) the process of frequency conversion is described by the overall Hamiltonian:

$$\hat{H}_{FC}(t) = \hat{H}_0^{(a)}(t) + \hat{H}_0^{(c)}(t) + \hat{H}_I^{(FC)}(t) \tag{7}$$

There are a variety of different constants involved in the definition of the frequency conversion Hamiltonian in (7) (see (1), (3), (5) and (6)). However most are dependent on the initial definitions of the interacting fields. In the remainder of this paper we merge all of them into a coupling value depicting the overall efficiency of the frequency conversion process rendering the presented calculations independent of individual notations.

## 4. FC: General properties

The frequency conversion Hamiltonian in (7) generates the unitary transformation

$$\hat{U}_{FC} = \mathcal{T} \exp\left[-\frac{\imath}{\hbar}\int \mathrm{d}t\, \hat{H}_{FC}(t)\right]. \tag{8}$$

In (8) the *time-ordering* operator $\mathcal{T}$ is crucial, because the electric field operators in $\hat{H}_{FC}(t)$ are time-dependent. In turn, the Hamiltonian does not commute at different points in time, which renders finding a solution difficult. The structure of (8) already gives valuable insights into the properties of the system. The Hamiltonian in (8) is bilinear in its electric field operators — the pump is treated as a classical wave — and the solution hence takes the form of a linear operator transformation [37, 38, 39].§ In the monochromatic picture the solution is of the form [18]:

$$\begin{aligned}
\hat{a}^{(out)}(\omega) &= \cos(r)\hat{a}^{(in)}(\omega) + \sin(r)\hat{c}^{(in)}(\omega')\\
\hat{c}^{(out)}(\omega') &= \cos(r)\hat{c}^{(in)}(\omega') - \sin(r)\hat{a}^{(in)}(\omega)
\end{aligned} \tag{9}$$

A single frequency $\hat{a}^{(in)}(\omega)$ has a certain conversion amplitude $\sin(r)$ which defines which part of the beam will be converted to $\hat{c}^{(out)}(\omega')$, via sum-frequency or difference frequency generation, whereas the rest is transmitted without change to $\hat{a}^{(out)}(\omega)$. This mathematical structure is very similar to the transmissivity and reflectivity of a beam-splitter [40]. In the frequency conversion case, however, not two spatial modes but two optical modes at different frequencies are coupled with each other.

This behavior is not immediately visible in the multimode regime, where we have to consider the conversion of many frequencies:

$$\begin{aligned}
\hat{a}^{(out)}(\omega) &= \int \mathrm{d}\omega' U_a(\omega,\omega')\,\hat{a}^{(in)}(\omega') + \int \mathrm{d}\omega' V_a(\omega,\omega')\,\hat{c}^{(in)}(\omega')\\
\hat{c}^{(out)}(\omega) &= \int \mathrm{d}\omega' U_c(\omega,\omega')\,\hat{c}^{(in)}(\omega') - \int \mathrm{d}\omega' V_c(\omega,\omega')\,\hat{a}^{(in)}(\omega')
\end{aligned} \tag{10}$$

Here the functions $U_{a/c}(\omega,\omega')$ in (10) define which parts of the different frequencies of the input beams pass the crystal unperturbed, whereas the $V_{a/c}(\omega,\omega')$ functions give the portions of the beams which are converted via sum frequency or difference frequency generation.

In order to unravel the underlying structure we use the constraint that the frequency conversion process is a unitary transformation and hence (10) has to form a canonical transformation [38, 39]. This imposes several conditions on the properties of the solution which we study in detail in Appendix A. Under this constraint and with the help of the Bloch-Messiah decomposition we rewrite (10) as

$$\begin{aligned}
\hat{A}_k^{(out)} &= \cos(r_k)\,\hat{A}_k^{(in)} + \sin(r_k)\,\hat{C}_k^{(in)}\\
\hat{C}_k^{(out)} &= \cos(r_k)\,\hat{C}_k^{(in)} - \sin(r_k)\,\hat{A}_k^{(in)},
\end{aligned} \tag{11}$$

where $\hat{A}_k$ and $\hat{C}_k$ are broadband single-photon destruction operators [41] defined as:

$$\begin{aligned}
\hat{A}_k^{(out)} &= \int \mathrm{d}\omega\, \varphi_k(\omega)\,\hat{a}^{(out)}(\omega) \qquad & \hat{C}_k^{(out)} &= \int \mathrm{d}\omega\, \xi_k(\omega)\,\hat{c}^{(out)}(\omega)\\
\hat{A}_k^{(in)} &= \int \mathrm{d}\omega\, \psi_k(\omega)\,\hat{a}^{(in)}(\omega) \qquad & \hat{C}_k^{(in)} &= \int \mathrm{d}\omega\, \phi_k(\omega)\,\hat{c}^{(in)}(\omega)
\end{aligned} \tag{12}$$

---

§ Solving the process via the Heisenberg equation of motion (see section 7), yields a linear operator valued differential equation. Linear operator valued differential equations are solved by linear Bogoliubov transformation, i.e. the solution will be of the form (10). Furthermore with the help of the Bloch-Messiah reduction, discussed in Appendix A, we are able to rewrite the general linear Bogoliubov transformation [39] into the form depicted in (11).

This means that broadband frequency conversion is equivalent to the transformation of an orthonormal set of optical pulses given by the broadband mode shapes in (12). Each individual pulse is, independently from the rest, partially converted and partially transmitted. According to (11) we consequently are able to regard the overall frequency conversion process as a quantum pulse gate [19, 18, 20] which, depending on the efficiency of the process, transmits the incoming pulses unperturbed or switches them via frequency conversion.

The crucial parameters of this transformation are firstly the conversion amplitudes $r_k$ which give the efficiency of the process — conversion efficiency $= \sin^2(r_k)$ — and secondly the broadband mode shapes $\varphi_k(\omega)$, $\xi_k(\omega)$, $\psi_k(\omega)$ and $\phi_k(\omega)$ that define the range of frequencies which are interconverted.

## 5. FC: Time-ordering approximation

In order to obtain some first insights into the frequency conversion process we use perturbation theory. In the case of a time-dependent Hamiltonian a Dyson series expansion is necessary [42]. This approach was studied in detail by Agata M. Brańczyk in [30] and [43]. Here we shortly recapitulate the general approach, starting with the Dyson series expansion of (8):

$$\begin{aligned}\hat{U}_{FC} &= \mathcal{T}\exp\left[-\frac{\imath}{\hbar}\int \mathrm{d}t\,\hat{H}_{FC}(t)\right]\\ &= \mathbb{1} - \frac{\imath}{\hbar}\int_{-\infty}^{\infty}\mathrm{d}t_1\,\hat{H}_{FC}(t_1)\\ &+ \left(\frac{\imath}{\hbar}\right)^2\int_{-\infty}^{\infty}\mathrm{d}t_1\,\hat{H}_{FC}(t_1)\int_{-\infty}^{t_1}\mathrm{d}t_2\,\hat{H}_{FC}(t_2) + \cdots \qquad (13)\end{aligned}$$

In our case we regard the system long after the interaction in the crystal has taken place and consequently use plus and minus infinity as the overall bounds for the time-integration.

Unfortunately it is not trivial to perform the Dyson series expansion for FC, because coupled time integrals appear. To simplify this evaluation we introduce the time-ordering approximation. Hereby we approximate (8) by ignoring the time-ordering operator $\mathcal{T}$. By dropping $\mathcal{T}$ in (8) a simple Taylor series expansion becomes sufficient:

$$\begin{aligned}\hat{U}_{FC} &= \exp\left[-\frac{\imath}{\hbar}\int \mathrm{d}t\,\hat{H}_{FC}(t)\right]\\ &= \mathbb{1} - \frac{\imath}{\hbar}\int_{-\infty}^{\infty}\mathrm{d}t_1\,\hat{H}_{FC}(t_1)\\ &+ \frac{1}{2}\left(\frac{\imath}{\hbar}\right)^2\int_{-\infty}^{\infty}\mathrm{d}t_1\,\hat{H}_{FC}(t_1)\int_{-\infty}^{\infty}\mathrm{d}t_2\,\hat{H}_{FC}(t_2) + \cdots \qquad (14)\end{aligned}$$

Note the differences in the integration ranges and the expansion coefficients in (13) and (14) when terms of second order and higher are considered.

To investigate the differences between the two approaches we explicitly calculate the perturbation series up to second order. For this purpose it is beneficial to work with the electric field operators of (1) in the $\omega$-representation [33]:

$$\hat{E}^{(+)}(z,t) = \hat{E}^{(-)\dagger}(z,t)$$

$$= \imath \left( \frac{\hbar}{4\pi\epsilon_0 c\, A\, n(\omega_0)} \right)^{\frac{1}{2}} \int \mathrm{d}\omega \, \sqrt{\omega} \exp\left[\imath(k(\omega)z - \omega t)\right] \hat{a}(\omega) \tag{15}$$

We also perform our calculations in the interaction picture, this means we move into a new reference frame where the effects of free propagation are not present and hence do not need to consider the free propagation Hamiltonians. Finally we assume a crystal featuring a constant $\chi^{(2)}$-nonlinearity extending from $-\frac{L}{2}$ to $\frac{L}{2}$. The frequency conversion Hamiltonian from (7) takes the form

$$\begin{aligned} \hat{H}^{(FC)}(t) &= \epsilon_0 \chi^{(2)} \int_{-\frac{L}{2}}^{\frac{L}{2}} \mathrm{d}z \, E_p^{(+)}(z, t_1) \hat{E}_a^{(+)}(z, t_1) \hat{E}_c^{(-)}(z, t_1) + h.c. \\ &= \epsilon_0 \chi^{(2)} L \int \mathrm{d}\omega_p \int \mathrm{d}\omega_a \int \mathrm{d}\omega_c \, \alpha(\omega_p) \, \mathrm{sinc}\left( \frac{\Delta k(\omega_p, \omega_a, \omega_c) L}{2} \right) \\ &\times \exp\left(-\imath \Delta\omega t\right) \hat{a}(\omega_a) \hat{c}^\dagger(\omega_c) + h.c. \end{aligned} \tag{16}$$

where we introduced the two abbreviations $\Delta k(\omega_p, \omega_a, \omega_c) = k_p(\omega_p) + k_a(\omega_a) - k_c(\omega_c)$ and $\Delta\omega = \omega_p + \omega_a - \omega_c$.

The approximations performed when ignoring time-ordering effects are located in the time-integrations in the term $\exp\left(-\imath\Delta\omega t\right)$. The time-integration of the first-order term gives identical results for both the Taylor and Dyson series expansion:

$$\int_{-\infty}^{\infty} \exp\left(-\imath \Delta\omega t\right) = 2\pi \delta(\Delta\omega) \tag{17}$$

From a physical point of view the obtained delta function $\delta(\Delta\omega)$ describes the energy conservation between the three interacting photons: the input, the pump, and the output photon.

In the second order expansion the time integrals in two perturbation approaches start to deviate from each other. The time-integration of the Taylor series in (14) yields

$$\begin{aligned} &\int_{-\infty}^{\infty} \mathrm{d}t_1 \int_{-\infty}^{\infty} \mathrm{d}t_2 \exp\left(-\imath \Delta\omega t_1\right) \exp\left(-\imath \Delta\omega' t_2\right) \\ &= \delta(\Delta\omega)\delta(\Delta\omega') \end{aligned} \tag{18}$$

which is just two times the result of the first-order expansion. In the Dyson series however we obtain a different result [30]:

$$\begin{aligned} &\int_{-\infty}^{\infty} \mathrm{d}t_1 \int_{-\infty}^{t_1} \mathrm{d}t_2 \, \exp\left[-\imath \Delta\omega t_1\right] \exp\left[-\imath \Delta\omega' t_2\right] \\ &= 2\pi^2 \, \delta(\Delta\omega + \Delta\omega') \left( \delta(\Delta\omega - \Delta\omega') + \frac{1}{\pi} \frac{1}{\Delta\omega - \Delta\omega'} \right) \end{aligned} \tag{19}$$

This term shows the crucial difference between the inclusion and the exclusion of time-ordering effects. When we exclude time-ordering effects the time-integrations in every order yield delta functions $\delta(\omega_p + \omega_a - \omega_c)$ between three different frequencies. We can interpret this mathematical expression by a physical process where only three photons interact with each other. This means that even in the case of a multitude of photon conversions take place in the overall process the energy is still conserved in each photon triplet. Effectively this means that the spectral properties of the interacting photons are identical in every order of the perturbation series.

This is quite different from the Dyson expansion. Here delta functions of the form $\delta(\Delta\omega + \Delta\omega')$ appear in the second-order expansion. From a physical point of view this delta function describes energy conservation which does not occur between the three but between six photons. Either the SFG (DFG) of two photons takes place simultaneously or a SFG (DFG) with successive DFG (SFG) conversion of a single-photon takes place.‖ This enables an enhanced flexibility in the available energy range and modifies the solution, especially its spectral properties, with respect to the Taylor expansion. Since the energy, in these terms, only has to be conserved for the *overall* process and not the individual photon triplets the constraints imposed by energy conservation are relaxed. A graphical representation of this effect in the third-order expansion is shown in figure 2.

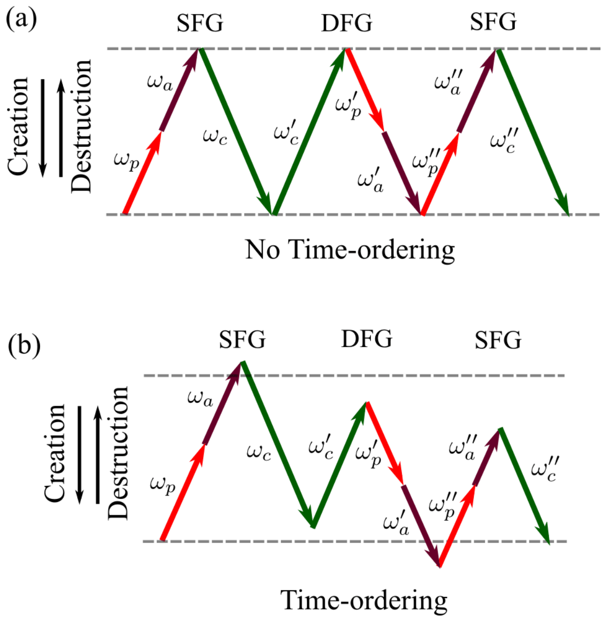

**Figure 2.** Schematic diagrams depicting the energy conservation during successive SFG and DFG processes neglecting time-ordering effects (Analytic model) (a) and including time-ordering (Rigorous model) (b). Neglecting time-ordering effects the energy is conserved between the three photons in each individual SFG/DFG process, whereas the rigorous model including time-ordering effects only requires energy conservation during the overall process [30].

The time-ordering approximation will consequently give accurate results as long as the conversion efficiency is not too high and the first-order perturbation expansion is the dominant term in the solution.

## 6. FC: Analytic model excluding time-ordering effects

The huge advantage of neglecting time-ordering effects in frequency conversion is the fact that it enables us to build an analytical model of frequency conversion, which is highly beneficial since it enables quick and straightforward access to the process properties:

---

‖ The individual orders $n$ of the perturbation expansion do not directly correspond to the conversion of $n$ photons, multiple back and forth conversions of a single-photon can appear as well. In order to obtain the full dynamics of the process all orders have to be considered.

$$\hat{U}_{FC} = \exp\left[-\frac{\imath}{\hbar}\int \mathrm{d}t\, \hat{H}_I^{(FC)}(t)\right] \tag{20}$$

This formula is identical to (8) except that we dropped the time-ordering operator $\mathcal{T}$ and work in the interaction picture. It enables us to directly perform the time-integration in the exponential function. As in the previous section we perform our calculations in the $\omega$-representation and again we assume a crystal featuring a constant $\chi^{(2)}$-nonlinearity extending from $-\frac{L}{2}$ to $\frac{L}{2}$. After a straightforward calculation we obtain

$$\begin{aligned}\int \mathrm{d}t\, \hat{H}_I^{(FC)}(t) = &\int \mathrm{d}t\, \epsilon_0 \chi^{(2)} \int_{-\frac{L}{2}}^{\frac{L}{2}} \mathrm{d}z\, E_p^{(+)}(z,t)\hat{E}_a^{(+)}(z,t)\hat{E}_c^{(-)}(z,t) + h.c.\\ &= B\int \mathrm{d}\omega_a \int \mathrm{d}\omega_c\, \alpha\left(\omega_c - \omega_a\right)\\ &\quad\times \operatorname{sinc}\left(\frac{\Delta k(\omega_a,\omega_c)L}{2}\right)\hat{a}(\omega_a)\hat{c}^\dagger(\omega_c) + h.c.\end{aligned} \tag{21}$$

where we merged all constants into the overall factor $B$ and $\Delta k(\omega_a,\omega_c) = k_p(\omega_c - \omega_a) + k_a(\omega_a) - k_c(\omega_c)$. Details of this calculation are given in [18]. Defining

$$f(\omega_a,\omega_c) = B\,\alpha\left(\omega_c - \omega_a\right)\operatorname{sinc}\left(\frac{\Delta k(\omega_a,\omega_c)L}{2}\right), \tag{22}$$

the unitary transformation generated by (20) takes on the form:

$$\hat{U}_{FC} = \exp\left[-\frac{\imath}{\hbar}\left(\int \mathrm{d}\omega_a \int \mathrm{d}\omega_c\, f(\omega_a,\omega_c)\hat{a}(\omega_a)\hat{c}^\dagger(\omega_c) + h.c.\right)\right] \tag{23}$$

With the help of the singular-value-decomposition theorem [44] we recast this solution in the broadband mode formalism presented in (11). At first we diagonalize the Hamiltonian by decomposing the exponent in (23), via a Schmidt decomposition, as:

$$\begin{aligned}-\frac{\imath}{\hbar}f(\omega_a,\omega_c) &= \sum_k (-r_k)\psi_k(\omega_a)\phi_k^*(\omega_c)\\ -\frac{\imath}{\hbar}f^*(\omega_a,\omega_c) &= \sum_k r_k\psi_k^*(\omega_a)\phi_k(\omega_c)\end{aligned} \tag{24}$$

Here both $\{\psi_k(\omega_a)\}$ and $\{\phi_k(\omega_c)\}$ each form a complete set of orthonormal functions and $r_k \in \mathcal{R}^+$. Employing equation (24) we rewrite the unitary frequency conversion transformation in (23) as:

$$\begin{aligned}\hat{U}_{FC} = \exp\Bigg[&\sum_k (-r_k)\int \mathrm{d}\omega_a\, \psi_k(\omega_a)\hat{a}(\omega_a)\int \mathrm{d}\omega_c \phi_k^*(\omega_c)\hat{c}^\dagger(\omega_c)\\ &+ r_k\int \mathrm{d}\omega_a \psi_k^*(\omega_a)\hat{a}^\dagger(\omega_a)\int \mathrm{d}\omega_c \phi_k(\omega_c)\hat{c}(\omega_c)\Bigg]\end{aligned} \tag{25}$$

With the help of the broadband mode operators defined in (12) it takes on the form

$$\begin{aligned}\hat{U}_{FC} &= \exp\left[\sum_k (-r_k)\left(\hat{A}_k\hat{C}_k^\dagger - \hat{A}_k^\dagger\hat{C}_k\right)\right]\\ &= \bigotimes_k \exp\left[(-r_k)\left(\hat{A}_k\hat{C}_k^\dagger - \hat{A}_k^\dagger\hat{C}_k\right)\right].\end{aligned} \tag{26}$$

The solution of (26) is well known and, in the Heisenberg pictures, it reads [37]:

$$\begin{aligned}\hat{A}_k^{(out)} &= \cos(r_k)\hat{A}_k^{(in)} + \sin(r_k)\hat{C}_k^{(in)}\\ \hat{C}_k^{(out)} &= \cos(r_k)\hat{C}_k^{(in)} - \sin(r_k)\hat{A}_k^{(in)}\end{aligned} \tag{27}$$

This simplified analytic model features exactly the structure required by the canonical commutation relations discussed in section 4. Only the additional fact that the input modes and output modes in this simplified model are always of identical shape differs from the general solution (11).

It is evident that this treatment ignoring time-ordering effects enables a straightforward analytic solution of the frequency conversion process. In contrast to the perturbation approach in section 5 we do not require to evaluate a perturbation series up to infinite order and, in some cases, even the SVD can be performed analytically and hence no computational effort is required at all [45]. This enables the efficient engineering and design of frequency conversion processes as long as the applied approximations hold.

## 7. FC: Rigorous theory including time-ordering effects

In order to obtain a rigorous solution of frequency conversion we have to include the effects of time-ordering and the corresponding relaxed energy conservation conditions into our calculations. For this purpose we change our analysis method and regard the frequency conversion process in the Heisenberg picture. This approach was already utilized for frequency conversion in nonlinear optical fibers in [14, 20] and is common for parametric down-conversion [32, 29, 27, 28, 46, 47, 48, 49, 50]. In order to solve the corresponding Heisenberg equations of motion we adapt the work of Mikhail I. Kolobov on PDC in [32] to frequency conversion. It enables the complete time-ordered solution of the frequency conversion process without having to perform the Dyson series expansion up to infinite orders. As a first step we redefine the electric field operators in (1) according to [32]

$$\hat{a}(z,t) = \frac{1}{\sqrt{2\pi k_0}} \int \mathrm{d}k \, \sqrt{\omega(k)} \exp\left[\imath\left(kz - \omega(k)t\right)\right] \hat{a}(k) \tag{28}$$

$$\hat{c}(z,t) = \frac{1}{\sqrt{2\pi k_0}} \int \mathrm{d}k \, \sqrt{\omega(k)} \exp\left[\imath\left(kz - \omega(k)t\right)\right] \hat{c}(k) \tag{29}$$

The Heisenberg equation of motion for $\hat{a}(z,t)$ reads:

$$\frac{d}{dt}\hat{a}(z,t) = \frac{\imath}{\hbar}\left[\hat{H}_{FC}(t), \hat{a}(z,t)\right] \tag{30}$$

We first calculate the commutator of $\hat{a}(z,t)$ with the free space Hamiltonian $\hat{H}_0^{(a,c)}(t)$. The commutation relation with the free space Hamiltonian $\hat{H}_0^{(c)}(t)$ directly results in zero whereas the commutator with $\hat{H}_0^{(a)}(t)$ yields [32]:

$$\begin{aligned}\frac{\imath}{\hbar}\left[\hat{H}_0^{(a)}(t), \hat{a}(z,t)\right] &= \frac{\imath}{\hbar}\left[\hbar k_0 \int \mathrm{d}z' \hat{a}^\dagger(z',t)\hat{a}(z',t), \hat{a}(z,t)\right]\\ &= \imath k_0 \int \mathrm{d}z' \ \left[\hat{a}^\dagger(z',t), \hat{a}(z,t)\right] \hat{a}(z',t)\end{aligned} \tag{31}$$

The crucial part in (31) is the commutator between the electric fields, at the same time, but at two different points in the medium:

$$\left[\hat{a}(z,t), \hat{a}^\dagger(z',t)\right] = \frac{1}{2\pi} \int \mathrm{d}k \, \frac{\omega(k)}{k_0} \exp\left[\imath k(z - z')\right] \tag{32}$$

In order to solve the integral in (32) we Taylor expand the dispersion relation up to first-order and obtain:

$$\begin{aligned}
&\left[\hat{a}(z,t),\hat{a}^\dagger(z',t)\right]\\
&=\frac{1}{2\pi}\frac{\omega_0}{k_0}\int \mathrm{d}k\,\left(1+\frac{k-k_0}{k_0}\right)\exp\left[\imath k(z-z')\right]\\
&=\frac{1}{2\pi}\frac{\omega_0}{k_0}\int \mathrm{d}k\,\frac{k}{k_0}\exp\left[\imath k(z-z')\right]\\
&=\frac{1}{2\pi}\frac{\omega_0}{k_0}\int \mathrm{d}k\,\frac{-\imath}{k_0}\frac{\partial}{\partial z}\exp\left[\imath k(z-z')\right]\\
&=\frac{-\imath}{k_0}\frac{c}{n_0}\frac{\partial}{\partial z}\delta(z-z')
\end{aligned}\tag{33}$$

Using (33) the free space commutation relation in (31) evaluates to:

$$\frac{\imath}{\hbar}\left[\hat{H}_0^{(a)}(t),\hat{a}(z,t)\right]=-\frac{c}{n_0}\frac{\partial}{\partial z}\hat{a}(z,t)\tag{34}$$

Next we calculate the commutator of $\hat{a}(z,t)$ with the nonlinear interaction Hamiltonian $\hat{H}_I^{(FC)}(t)$ in (6). To simplify this problem we treat $\omega(k)$ as a constant $\omega(k_0)$ using the slowly varying amplitude approximation. The commutator consequently evaluates to a delta function:

$$\left[\hat{a}(z,t),\hat{a}^\dagger(z',t)\right]=\frac{c}{n_0}\delta(z-z')$$

We obtain:

$$\begin{aligned}
&\frac{\imath}{\hbar}\left[\hat{H}_I^{(FC)}(t),\,\hat{a}(z,t)\right]=\\
&=\frac{\imath}{\hbar}\left[D\int \mathrm{d}z'\,E_p^{(+)}(z',t)\hat{a}(z',t)\hat{c}^\dagger(z',t)+h.c.\,,\hat{a}(z,t)\right]\\
&=\frac{\imath}{\hbar}D^*\int \mathrm{d}z'\,\left[\hat{a}^\dagger(z',t),\hat{a}(z,t)\right]E_p^{(-)}(z',t)\,\hat{c}(z',t)\\
&=\frac{\imath}{\hbar}D^*\int \mathrm{d}z'\,E_p^{(-)}(z',t)\,\hat{c}(z',t)\left(-\frac{c}{n_0}\right)\delta(z-z')\\
&=-\frac{\imath}{\hbar}\frac{c}{n_0}D^*\,E_p^{(-)}(z,t)\,\hat{c}(z,t)
\end{aligned}\tag{35}$$

Here we merged all constants into the overall variable $D$. The Heisenberg equation of motion in (30) then reads:

$$\frac{d}{dt}\hat{a}(z,t)=-\frac{c}{n_0}\frac{\partial}{\partial z}\hat{a}(z,t)-\frac{\imath}{\hbar}\frac{c}{n_0}D^*E_p^{(-)}(z,t)\hat{c}(z,t)\tag{36}$$

Since we are interested in the spectral distribution of the output we perform a Fourier transformation into the frequency domain. We regard the created electric fields long after the interaction and therefore integrate the time dependence from minus to plus infinity, as already performed in the analytic solution in section 6:

$$\begin{aligned}
\mathcal{F}\left[\frac{d}{dt}\hat{a}(z,t)\right]&=\mathcal{F}\left[-\frac{c}{n_0}\frac{\partial}{\partial z}\hat{a}(z,t)\right]-\frac{\imath}{\hbar}\frac{c}{n_0}\mathcal{F}\left[D^*E_p^{(-)}(z,t)\hat{c}(z,t)\right]\\
-\imath\omega\hat{a}(z,\omega)&=-\frac{c}{n_0}\frac{\partial}{\partial z}\hat{a}(z,\omega)-\frac{\imath}{\hbar}\frac{c}{n_0}D^*\int \mathrm{d}\omega' E_p^{(-)}(z,\omega'-\omega)\hat{c}(z,\omega')
\end{aligned}\tag{37}$$

We further separate the interaction from the propagation effects by transforming our operators into the interaction picture, similar to the analytic solution in section 6. For this purpose we introduce the electric fields:

$$\begin{aligned}
&\hat{\epsilon}_a(z,\omega) = \hat{a}(z,\omega)\exp\left[-\imath k_a(\omega) z\right]\\
&\hat{\epsilon}_c(z,\omega) = \hat{c}(z,\omega)\exp\left[-\imath k_c(\omega) z\right]\\
&\epsilon_p^{(-)}(z,\omega) = E_p^{(-)}(z,\omega)\exp\left[\imath k_p(\omega) z\right]
\end{aligned} \tag{38}$$

With the help of (38) we transform the differential equation in (37) into the interaction picture:

$$\begin{aligned}
\frac{\partial}{\partial z}\hat{\epsilon}_a(z,\omega) = &-\frac{\imath}{\hbar}D^*\int \mathrm{d}\omega'\epsilon_p^{(-)}(z,\omega'-\omega)\hat{\epsilon}_c(z,\omega')\\
&\times\exp\left\{-\imath\left[k_p(\omega'-\omega)-k_c(\omega')+k_a(\omega)\right]z\right\}
\end{aligned} \tag{39}$$

In a similar manner we calculate the differential equation of the second beam and obtain:

$$\begin{aligned}
\frac{\partial}{\partial z}\hat{\epsilon}_c(z,\omega) = &-\frac{\imath}{\hbar}D\int \mathrm{d}\omega'\epsilon_p^{(+)}(z,\omega-\omega')\hat{\epsilon}_a(z,\omega')\\
&\exp\left\{\imath\left[k_p(\omega-\omega')+k_a(\omega')-k_c(\omega)\right]z\right\}
\end{aligned} \tag{40}$$

Finally we introduce the abbreviation $\Delta k(\omega,\omega') = k_p(\omega'-\omega) - k_c(\omega') + k_a(\omega)$. The two coupled differential equations describing the frequency conversion process read:

$$\begin{aligned}
&\frac{\partial}{\partial z}\hat{\epsilon}_a(z,\omega) = -\frac{\imath}{\hbar}D^*\int \mathrm{d}\omega'\epsilon_p^{(-)}(z,\omega'-\omega)\exp\left[-\imath\Delta k(\omega,\omega')z\right]\hat{\epsilon}_c(z,\omega')\\
&\frac{\partial}{\partial z}\hat{\epsilon}_c(z,\omega) = -\frac{\imath}{\hbar}D\int \mathrm{d}\omega'\epsilon_p^{(+)}(z,\omega-\omega')\exp\left[\imath\Delta k(\omega',\omega)z\right]\hat{\epsilon}_a(z,\omega')
\end{aligned} \tag{41}$$

Note the inversion of the $\omega$ and $\omega'$ factors in the $\Delta k$ and $\epsilon_p$ functions between the two formulas. By defining

$$f(\omega,\omega',z) = -\frac{\imath}{\hbar}D^*\epsilon_p^{(-)}(z,\omega'-\omega)\exp\left[-\imath\Delta k(\omega,\omega')z\right] \tag{42}$$

we may write (41) in a more compact notation:

$$\begin{aligned}
&\frac{\partial}{\partial z}\hat{\epsilon}_a(z,\omega) = \int \mathrm{d}\omega' f(\omega,\omega',z)\,\hat{\epsilon}_c(z,\omega')\\
&\frac{\partial}{\partial z}\hat{\epsilon}_c(z,\omega) = -\int \mathrm{d}\omega' f^*(\omega',\omega,z)\,\hat{\epsilon}_a(z,\omega')
\end{aligned} \tag{43}$$

### *7.1. Solving the differential equations*

In order to obtain the dynamics of the frequency conversion process the differential equations in (43) have to be solved. Usually operator valued differential equations cannot readily be evaluated and, in the case of FC, this is complicated by the fact that we have to solve integro-differential equations, since we consider the conversion of many frequencies simultaneously. Note, that (41) is linear in its operators and hence classical solution methods like the split-step Fourier inversion method have been applied [20, 27, 28]. In the special case of a cw-pump laser the integral in (41) vanishes and it is even possible to find analytic solutions [32].

In this paper we apply a different approach — introduced by Wolfgang Mauerer in [46] — exploiting the fact that the structure of the solution is already known: it is a linear operator transformation (10). Using (10) and (43) we obtain two pairs of classical integro-differential equations [29]

$$\begin{aligned}\frac{\partial}{\partial z}U_a(z,\omega,\omega'') &= -\int \mathrm{d}\omega' f(\omega,\omega',z)V_c(z,\omega',\omega'')\\ \frac{\partial}{\partial z}V_c(z,\omega,\omega'') &= \int \mathrm{d}\omega' f^*(\omega',\omega,z)U_a(z,\omega',\omega'')\end{aligned} \tag{44}$$

and

$$\begin{aligned}\frac{\partial}{\partial z}U_c(z,\omega,\omega'') &= -\int \mathrm{d}\omega' f^*(\omega',\omega,z)V_a(z,\omega',\omega'')\\ \frac{\partial}{\partial z}V_a(z,\omega,\omega'') &= \int \mathrm{d}\omega' f(\omega,\omega',z)U_c(z,\omega',\omega'')\end{aligned} \tag{45}$$

which cover the complete dynamics of the frequency conversion process.

We solve these coupled integro-differential equations using an iterative approach. For the pair in (44) this means we first formally integrate both differential equations along $z$, where we assume a medium of length $L$, as in in the analytic solution discussed in section 6,

$$\begin{aligned}U_a(z,\omega,\omega'') &= \delta(\omega-\omega') - \int_{-\frac{L}{2}}^{\frac{L}{2}} \mathrm{d}z \int \mathrm{d}\omega' f(\omega,\omega',z)V_c(z,\omega',\omega'')\\ V_c(z,\omega,\omega'') &= \int_{-\frac{L}{2}}^{\frac{L}{2}} \mathrm{d}z \int \mathrm{d}\omega' f^*(\omega',\omega,z)U_a(z,\omega',\omega'').\end{aligned} \tag{46}$$

Here we also included our knowledge about the initial solution. If no interaction takes place the process is described by the identity operation $\hat{a}^{(out)}(\omega) = \hat{a}^{(in)}(\omega)$ and $\hat{c}^{(out)}(\omega) = \hat{c}^{(in)}(\omega)$ from which follows:

$$\begin{aligned}&U_a(z,\omega,\omega'') = U_c(z,\omega,\omega'') = \delta(\omega-\omega'')\\ &V_a(z,\omega,\omega'') = V_c(z,\omega,\omega'') = 0\end{aligned} \tag{47}$$

Starting with the initial solution for $U_a(z,\omega,\omega'')$ we then perform the two integrations in (46) and obtain a preliminary $V_c(z,\omega,\omega'')$. This is then used to obtain a new $U_a(z,\omega,\omega'')$. We repeat this iterative procedure till the functions converge.

The same method is applied to the second set of differential equations defining $U_c(z,\omega,\omega'')$ and $V_a(z,\omega,\omega'')$ which gives us the complete time-ordered solution of the frequency conversion process. The implementation of this algorithm is discussed in Appendix D, where we also elaborate on the numerical accuracy of the applied method. The program code is available on our website.¶

## 8. FC: Comparison between simplified analytical and rigorous approach

In sections 6 and 7 we presented two models describing frequency conversion taking into account the higher-order moments: a simplified analytic model excluding time-ordering effects and a rigorous numerical model including time-ordering. While the analytic method is straightforward and only requires minimal computational effort, it is only an approximation to the rigorous model. In this section we compare these two approaches in order to investigate the validity of the simplified theory for the modelling of frequency conversion processes and the effects of time-ordering present in the rigorous solution.

---

¶ The program code can be downloaded from the publications section on our website. The current url is `http://physikwww.uni-paderborn.de/ag/ag-silberhorn/publications.html`.

From the discussion in section 6 we are able to directly deduce that the analytic solution features constant mode shapes connected to conversion amplitudes which oscillate with a sinusoidal pattern. In the low gain regime, when a first-order expansion is sufficient, the rigorous solution of section 7 gives the identical result. However, as soon as the higher-order moments yield a significant contribution to the frequency conversion process, the rigorous solution will feature a reshaped frequency spectrum due to the relaxed energy conservation condition discussed in section 5.

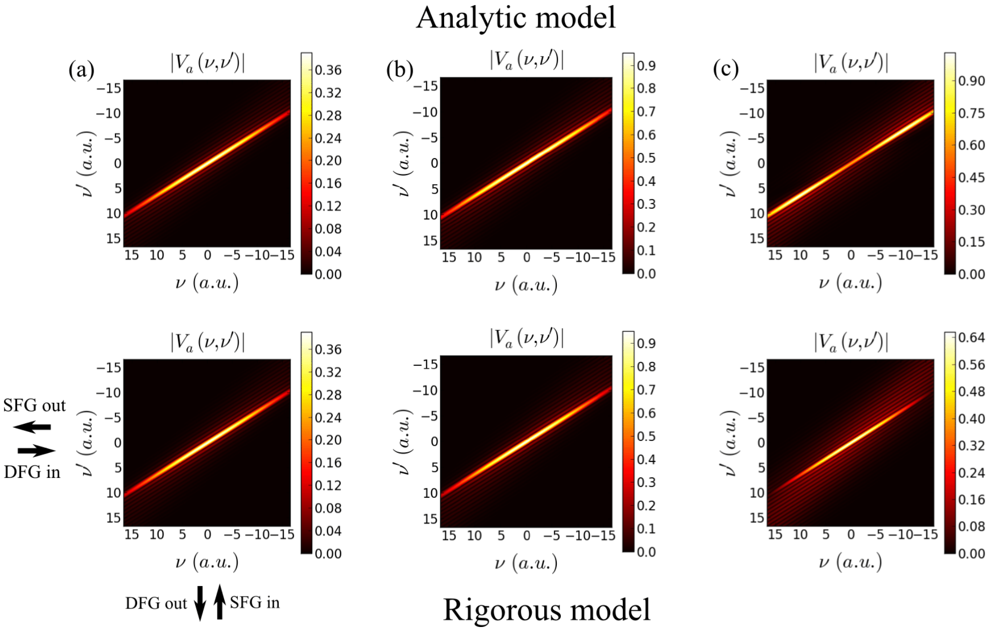

**Figure 3.** Comparison of the conversion amplitudes $|V_a(\omega,\omega')|$ between the rigorous and the simplified analytical model of a correlated frequency conversion process, with rising conversion efficiencies from (a) to (c). For low conversion efficiencies depicted in (a) both models yield identical results. When conversion efficiencies of unity are approached in (b) the rigorous model starts to deviate from the analytic approach due to the relaxed energy conservation condition. Significant differences occur when conversion efficiencies beyond unity are considered (c).

In order to quantify the discrepancies between the two approaches we simulate two frequency conversion processes: a correlated frequency conversion where many optical modes $r_k$ are converted and an almost uncorrelated frequency conversion process where only a few optical modes $r_k$ are present [18]. The frequency conversion process is defined by the incoming pump laser and the applied nonlinear crystal, i.e. the length of the material and its dispersion properties. These parameters can be represented by just six values: The length of the crystal, the group velocities of the three beams and the width and the amplitude of the Gaussian pump beam of our ultrafast laser system driving the frequency conversion process. The details of this procedure and the applied process properties are given in Appendix C.

The crucial parameter in the solution are the $\left|V_{a/c}(\omega,\omega')\right|$ amplitudes in the

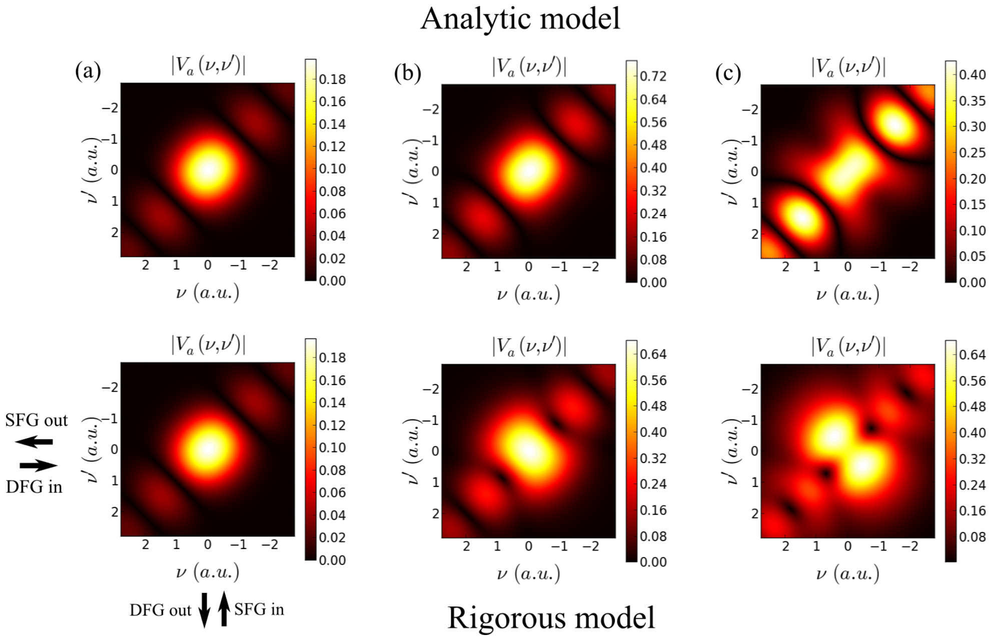

**Figure 4.** Comparison of the conversion amplitudes $|V_a(\omega,\omega')|$ between the rigorous and the simplified analytical model of an uncorrelated frequency conversion process, with rising conversion efficiencies from (a) to (c). For low conversion efficiencies in depicted in (a) both models yield identical results. When conversion efficiencies of unity are approached in (b) the rigorous model starts to deviate from the analytic approach due to the relaxed energy conservation condition. Significant differences occur when conversion efficiencies beyond unity are considered (c).

general solution in (10) which describe the conversion amplitude — conversion efficiency = $|\text{conversion amplitude}|^2$ — at individual frequencies. The $|V_a(\omega,\omega')|$ amplitudes for the correlated frequency conversion case are presented in figure 3. Figure 3(a) gives $|V_a(\omega,\omega')|$ at a low conversion rate. In this regime both models yield identical results. At efficiencies approaching unity, as depicted in figure 3 (b), minor deviations between the two models appear. Figure 3 (c) shows $|V_a(\omega,\omega')|$ for a conversion efficiency beyond unity. In this regime the time-ordering approximation breaks down and the two theories predict significantly different results. While the analytic model predicts a dip in the conversion efficiency about the central frequencies, the rigorous model still shows a Gaussian shape.

For the case of uncorrelated frequency conversion the $|V_a(\omega,\omega')|$ amplitudes are given in figure 4. As in the correlated case 4 (a) presents the process at low conversion efficiencies where both models are identical, (b) depicts near unit conversion efficiency with minor deviations between the two approaches and (c) visualizes the discrepancies between the two models arising at conversion rates beyond unity. In this uncorrelated frequency conversion case the discrepancies between the different models are much more prominent than in the correlated frequency conversion case. In the analytic model the side peaks are much more prominent as in the rigorous model. Furthermore the rigorous model shows a broadening and along the +45° axis, which is a direct result of the relaxed energy conservation conditions in this model.

The corresponding frequency conversion amplitudes $\sin(r_k)$ and mode shapes are displayed in figure 5 for correlated and in figure 6 for uncorrelated frequency conversion. The figures in the column on the left show the conversion amplitudes $\sin(r_k)$ — conversion efficiency $= \sin^2(r_k)$ — whereas the two columns on the right present the corresponding mode functions $\varphi_1(\nu), \psi_1(\nu), \phi_1(\nu)$ and $\xi_1(\nu)$ for the first optical mode featuring the highest conversion efficiency, where $\varphi_1(\nu)$ and $\psi_1(\nu)$ as well as $\phi_1(\nu)$ and $\xi_1(\nu)$ are of identical shape.

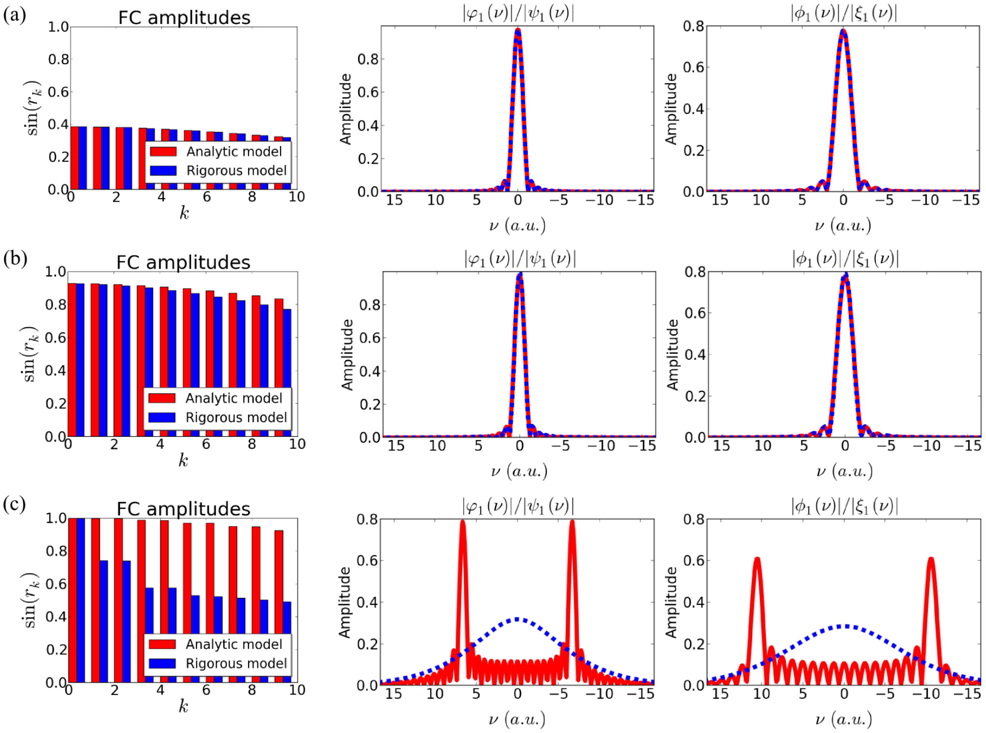

**Figure 5.** Comparison between the rigorous and the analytical approach in correlated many mode ultrafast frequency conversion. In the low conversion regime, presented in (a) (15%/15% conversion efficiency in the first mode in the analytic / rigorous model), both approaches evaluate to identical results. Approaching unit efficiency in (b) (86%/86% conversion efficiency in the first mode) the two approaches start to show differences, which become significant when optical gains beyond unity are considered in (c). (100%/99% conversion efficiency in the first mode)

In the conversion regime up to unity (a) both approaches yield almost identical conversion amplitudes $\sin(r_k)$ and corresponding mode functions $\varphi_1(\nu), \psi_1(\nu), \phi_1(\nu)$ and $\xi_1(\nu)$. At conversion rates about unity minor discrepancies in the mode shapes and $\sin(r_k)$ amplitudes start to appear. Significant differences between the two theories, however, are only present when we consider rates beyond unit conversion efficiency as depicted in (c).

Interestingly the time-ordering effects affect the correlated and uncorrelated frequency conversion in a different manner: in the correlated case the rigorous

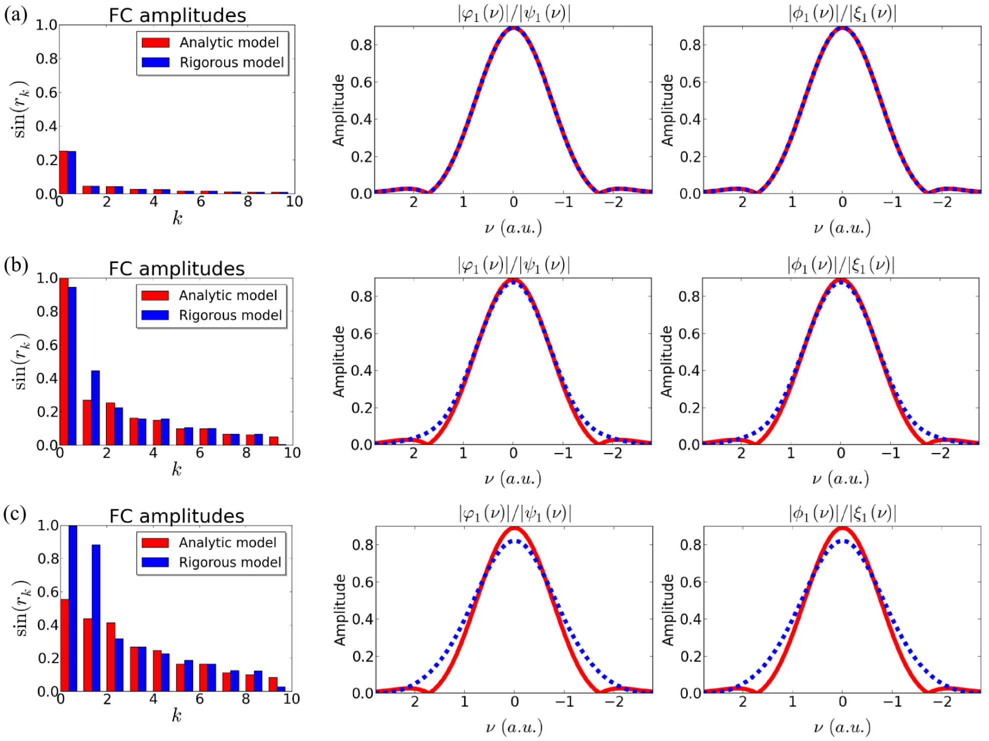

**Figure 6.** Comparison between the rigorous and the analytical approach in uncorrelated few mode ultrafast frequency conversion. In the low conversion regime, presented in (a), both approaches evaluate to identical results (6.4%/6.3% conversion efficiency in the first mode in the analytic / rigorous model). Approaching unit efficiency in (b) the two approaches start to show differences (100%/89% conversion efficiency in the first mode), which become significant when optical gains beyond unity are considered in (c) (30%/99% conversion efficiency in the first mode).

model predicts a considerably faster drop of the conversion amplitudes $\sin(r_k)$ than the analytical approach. Diamentral to this behaviour the $\sin(r_k)$ amplitudes of decorrelated case in the rigorous model, presented in 6(c), remain at unit conversion efficiency once they reach this value. In general it is not possible to associate the time-ordering effects with a specific behaviour of the broadband conversion amplitudes $\sin(r_k)$. Consequently each frequency conversion process has to be investigated individually.

Both correlated and uncorrelated down-conversion, however, share the property that the rigorous model predicts a significant broadening in the corresponding mode shapes in the high gain regime. Please note, that in figure 5 (c) the first mode of the analytic model is not the Gaussian from 5 (a) and (b) any more since we always plot the modes with the highest conversion efficiency and, in this power regime, this is not a Gaussian any more.

In summary the analytical model accurately describes frequency conversion in the low gain regime up to unit conversion efficiency, where minor deviations start to appear. Only in the high gain regime, when conversion efficiencies beyond unity are reached, complicated non-trivial deviations from the analytical model have to be taken into account and a rigorous treatment of frequency conversion is required. For most experimental setups and applications it is hence perfectly justified to apply the simplified analytic model to minimize the computational effort, as long as its limitations are kept in mind.

## 9. FC: Outlook

These time-ordering effects have practical implications for the deployment of frequency conversion processes. Especially affected are frequency conversion processes which serve as quantum pulse gates [18, 19, 20]. In theory a perfect quantum pulse gate converts a single optical mode with unit efficiency. Actually building a quantum pulse gate, however, is complicated by time-ordering effects. As is evident from figure 6 the relaxed energy conditions move the frequency process from the single-mode regime towards a more multimode behaviour. This effect fundamentally limits the gate performance at high conversion efficiencies. One could, in principle, use advanced engineering techniques, such as hypergrating structures to reduce the amount of multimodeness in the state [51], yet still the time-ordering effects seem to remain a fundamental limitation. Whether or not it is actually possible to engineer single-mode pulse gates including the effects of time-ordering remains an open research question.

## 10. PDC: Overview

Having discussed frequency conversion we now extend our investigations to the second important nonlinear optical process: parametric down-conversion. The principle of PDC is sketched in figure 7. A strong pump beam decays inside a nonlinear optical material into two beams commonly labelled signal and idler. The output state formed by the two beams is known as finitely squeezed EPR-state or twin-beam state[+]. As in the frequency conversion case, we do not restrict ourselves to a discussion of the parametric down-conversion process in the monochromatic picture, but extend the theories to the multimode picture including the interaction of many frequencies. This is especially important when the PDC process is pumped by pulsed laser systems.

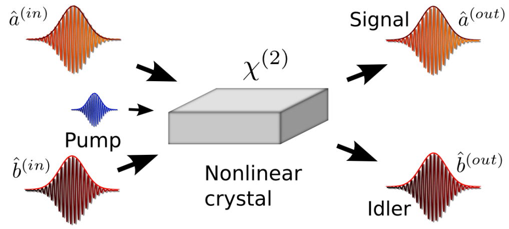

**Figure 7.** Sketch of the parametric down-conversion process. A strong pump beam decays inside the nonlinear optical material into two beams usually labelled signal $\hat{a}$ and idler $\hat{b}$, forming a finitely squeezed EPR-state.

---

[+] PDC is also able to create squeezed states. This process is discussed in [27, 28].

## 11. PDC: Hamiltonian

The interaction Hamiltonian of the PDC process — using electric field operators as defined in (1) and the rotating wave approximation — takes on the form:

$$\hat{H}_I^{(PDC)}(t) = \epsilon_0 \int \mathrm{d}z\, \chi^{(2)}(z)\, \hat{E}_p^{(+)}(z,t)\hat{E}_a^{(-)}(z,t)\hat{E}_b^{(-)}(z,t) + h.c.\,. \tag{48}$$

As in the frequency conversion process we assume a strong pump field exceeding the amplitudes of the signal and idler fields by several orders of magnitude and hence treat it as a classical field propagating undepleted through the medium (see (5)). This transforms the interaction Hamiltonian to:

$$\hat{H}_I^{(PDC)}(t) = \epsilon_0 \int \mathrm{d}z\, \chi^{(2)}(z)\, E_p^{(+)}(z,t)\hat{E}_a^{(-)}(z,t)\hat{E}_b^{(-)}(z,t) + h.c.\,. \tag{49}$$

Using the free space propagation Hamiltonian from (3) and the interaction Hamiltonian from (49) the process of parametric downconversion is given by the overall Hamiltonian:

$$\hat{H}_{PDC}(t) = \hat{H}_0^{(a)}(t) + \hat{H}_0^{(b)}(t) + \hat{H}_I^{(PDC)}(t) \tag{50}$$

While, at first glance, the process of parametric down-conversion seems very different from the process of frequency conversion, comparing the interaction Hamiltonian of PDC in (49) and FC in (6) reveals that they both feature bilinear Hamitonians — the pump is treated as a classical field — with an almost identical structure and hence share many mathematical properties.

It is therefore straightforward to extend our presented calculations corresponding frequency conversion to parametric down-conversion. In order to avoid repetition we are going to only state the results and elaborate on the differences and similarities to the process of frequency conversion. The detailed calculations will be presented in [52].

## 12. PDC: General properties

The general solution of (50) takes on the form of a linear operator transformation [38, 39]:

$$\begin{aligned}
\hat{a}^{(out)}(\omega) &= \int \mathrm{d}\omega' U_a(\omega,\omega')\, \hat{a}^{(in)}(\omega') + \int \mathrm{d}\omega' V_a(\omega,\omega')\, \hat{b}^{(in)\dagger}(\omega') \\
\hat{b}^{(out)}(\omega) &= \int \mathrm{d}\omega' U_b(\omega,\omega')\, \hat{b}^{(in)}(\omega') + \int \mathrm{d}\omega' V_b(\omega,\omega')\, \hat{a}^{(in)\dagger}(\omega')
\end{aligned} \tag{51}$$

This solution is constrained by the fact that it has to form a canonical transformation [38, 39, 27]. Under this restriction we are able to rewrite it as:

$$\begin{aligned}
\hat{A}_k^{(out)} &= \cosh(r_k)\hat{A}_k^{(in)} + \sinh(r_k)\hat{B}_k^{(in)\dagger} \\
\hat{B}_k^{(out)} &= \cosh(r_k)\hat{B}_k^{(in)} + \sinh(r_k)\hat{A}_k^{(in)\dagger}
\end{aligned} \tag{52}$$

where $\hat{A}_k$ and $\hat{B}_k$ are defined as broadband single-photon destruction operators [41]:

$$\begin{aligned}
\hat{A}_k^{(out)} &= \int \mathrm{d}\omega\, \varphi_k(\omega)\, \hat{a}^{(out)}(\omega) \qquad & \hat{B}_k^{(out)} &= \int \mathrm{d}\omega\, \xi_k(\omega)\, \hat{b}^{(out)}(\omega) \\
\hat{A}_k^{(in)} &= \int \mathrm{d}\omega\, \psi_k(\omega)\, \hat{a}^{(in)}(\omega) \qquad & \hat{B}_k^{(in)} &= \int \mathrm{d}\omega\, \phi_k(\omega)\, \hat{b}^{(in)}(\omega)
\end{aligned} \tag{53}$$

The details of this procedure are given in Appendix B.

According to (52) the parametric downconversion process is a broadband twin-beam squeezer transformation. However, not a single finitely squeezed EPR state, but a multitude of twin beam states are emitted into broadband ultrafast pulse modes $\hat{A}_k$ and $\hat{B}_k$. The crucial parameters of this transformation are firstly the amplitudes $r_k$ which give both the amount of generated EPR entanglement — squeezing[dB] $= -10\log_{10}\left(e^{-2r_k}\right)$ — and the number of emitted EPR states, and secondly the mode shapes $\varphi_k(\omega)$, $\xi_k(\omega)$, $\psi_k(\omega)$, and $\phi_k(\omega)$ which define the form of the optical modes in which the states are created.

## 13. PDC: Time-ordering approximation

To obtain some first insights into the parametric down-conversion process given by (50) we applied perturbation theory, as performed in the case of frequency conversion, discussed in section 5. The mathematics are identical to the ones presented in section 5. Including time-ordering and performing a Dyson series expansion is involved yet gives an enhanced flexibility in the energy conservation condition, whereas neglecting time-ordering enables a straightforward Taylor expansion. An extensive discussion of Dyson series vs. Taylor series for PDC was performed by Agata M. Brańczyk in [30] and [43].

## 14. PDC: Analytic model excluding time-ordering effects

As in the frequency conversion case, presented in section 6, we first solve the process excluding time-ordering effects. Again we use the electric fields in the frequency domain (15) and move into the interaction picture:

$$\hat{U}_{PDC} = \exp\left[-\frac{\imath}{\hbar}\int \mathrm{d}t\, \hat{H}_I^{(PDC)}(t)\right] \tag{54}$$

Retracting the steps from section 6 we obtain

$$\hat{U}_{PDC} = \exp\left[-\frac{\imath}{\hbar}\left(\int \mathrm{d}\omega_a \int \mathrm{d}\omega_b\, f(\omega_a,\omega_b)\hat{a}^\dagger(\omega_a)\hat{b}^\dagger(\omega_b) + h.c.\right)\right], \tag{55}$$

where $f(\omega_a,\omega_b)$ is defined as

$$f(\omega_a,\omega_b) = B\,\alpha(\omega_a+\omega_b)\,\mathrm{sinc}\left(\frac{\Delta k(\omega_a,\omega_b)L}{2}\right) \tag{56}$$

and $\Delta k(\omega_a,\omega_b) = k_p(\omega_a+\omega_b) - k_a(\omega_a) - k_b(\omega_b)$.

In the broadband mode formalism this process evaluates to

$$\begin{aligned}\hat{U}_{PDC} &= \exp\left[\sum_k r_k\left(\hat{A}_k^\dagger\hat{B}_k^\dagger - \hat{A}_k\hat{B}_k\right)\right] \\ &= \bigotimes_k \exp\left[r_k\left(\hat{A}_k^\dagger\hat{B}_k^\dagger - \hat{A}_k\hat{B}_k\right)\right] = \bigotimes_k \hat{S}_k^{ab}(-r_k)\end{aligned} \tag{57}$$

which, in the Heisenberg formalism (57), takes on the form:

$$\begin{aligned}\hat{A}_k^{(out)} &= \cosh(r_k)\hat{A}_k^{(in)} + \sinh(r_k)\hat{B}_k^{\dagger(in)} \\ \hat{B}_k^{(out)} &= \cosh(r_k)\hat{B}_k^{(in)} + \sinh(r_k)\hat{A}_k^{\dagger(in)}\end{aligned} \tag{58}$$

The details of this calculation are given in [12].

This result exhibits exactly the structure imposed by the canonical commutation relation in (52), except for the fact that, as in the frequency conversion case, the input and output modes are of identical shape.

In conclusion the analytic model ignoring time-ordering effects enables a straightforward solution of the parametric down-conversion process, which enables the efficient engineering and design of frequency conversion processes as long as the applied approximations hold.

## 15. PDC: Rigorous theory including time-ordering effects

Having elaborated on solving parametric down-conversion neglecting time-ordering effects we now explicitly include these effects into our analysis. For this purpose we adapt the approach presented in section 7. We first define new electric field operators according to [32]

$$\begin{aligned}\hat{a}(z,t) &= \frac{1}{\sqrt{2\pi k_0}}\int \mathrm{d}k\,\sqrt{\omega(k)}\exp\left[\imath\left(kz-\omega(k)t\right)\right]\hat{a}(k)\\ \hat{b}(z,t) &= \frac{1}{\sqrt{2\pi k_0}}\int \mathrm{d}k\,\sqrt{\omega(k)}\exp\left[\imath\left(kz-\omega(k)t\right)\right]\hat{b}(k).\end{aligned} \tag{59}$$

In terms of (59) the Heisenberg equation of motion for $\hat{a}(z,t)$ takes on the form:

$$\frac{d}{dt}\hat{a}(z,t) = \frac{\imath}{\hbar}\left[\hat{H}_{PDC}(t),\hat{a}(z,t)\right] \tag{60}$$

Repeating exactly the same steps as in section 7 we obtain two operator valued integro-differential equations describing the downconversion process

$$\begin{aligned}\frac{\partial}{\partial z}\hat{\epsilon}_a(z,\omega) &= -\frac{\imath}{\hbar}D\int \mathrm{d}\omega'\exp\left[\imath\Delta k(\omega,\omega')z\right]E_p^{(+)}(z,\omega+\omega')\,\hat{\epsilon}_b^{\dagger}(z,\omega')\\ \frac{\partial}{\partial z}\hat{\epsilon}_b(z,\omega) &= -\frac{\imath}{\hbar}D\int \mathrm{d}\omega'\exp\left[\imath\Delta k(\omega',\omega)z\right]E_p^{(+)}(z,\omega+\omega')\,\hat{\epsilon}_a^{\dagger}(z,\omega')\end{aligned} \tag{61}$$

where we introduced the shorthand $\Delta k(\omega,\omega') = k_p(\omega+\omega') - k_a(\omega) - k_b(\omega')$. The structure of this result is very similar to the equations derived by [29, 46, 27] which serves as a nice cross check of our calculations. Also please take note of the switch of $\omega$ and $\omega'$ in the second equation.

By defining

$$f(\omega,\omega',z) = -\frac{\imath}{\hbar}DE_p^{(+)}(z,\omega+\omega')\exp\left[\imath\Delta k(\omega,\omega')z\right] \tag{62}$$

we rewrite the differential equations in a compact form:

$$\begin{aligned}\frac{\partial}{\partial z}\hat{\epsilon}_a(z,\omega) &= \int \mathrm{d}\omega' f(\omega,\omega',z)\,\hat{\epsilon}_b^{\dagger}(z,\omega')\\ \frac{\partial}{\partial z}\hat{\epsilon}_b(z,\omega) &= \int \mathrm{d}\omega' f(\omega',\omega,z)\,\hat{\epsilon}_a^{\dagger}(z,\omega')\end{aligned} \tag{63}$$

### *15.1. Solving the differential equations*

Since the structure of the two differential equations describing the PDC process in (63) is identical to the ones describing the frequency conversion process (41) and (43), we apply the same solution method as presented in section 7.1.

We obtain four classical integro-differential equations. Two for $U_a(z,\omega,\omega')$ and $V_b(z,\omega,\omega')$:

$$\begin{aligned} \frac{\partial}{\partial z}U_a(z,\omega,\omega'') &= \int \mathrm{d}\omega' f(\omega,\omega',z)V_b^*(z,\omega',\omega'') \\ \frac{\partial}{\partial z}V_b(z,\omega,\omega'') &= \int \mathrm{d}\omega' f(\omega',\omega,z)U_a^*(z,\omega',\omega'') \end{aligned} \tag{64}$$

And two for $U_b(z,\omega,\omega')$ and $V_a(z,\omega,\omega')$:

$$\begin{aligned} \frac{\partial}{\partial z}U_b(z,\omega,\omega'') &= \int \mathrm{d}\omega' f(\omega',\omega,z)V_a^*(z,\omega',\omega'') \\ \frac{\partial}{\partial z}V_a(z,\omega,\omega'') &= \int \mathrm{d}\omega' f(\omega,\omega',z)U_b^*(z,\omega',\omega'') \end{aligned} \tag{65}$$

The initial conditions are:

$$\begin{aligned} &U_a(z,\omega,\omega'') = U_b(\omega,\omega'',z) = \delta(\omega-\omega'') \\ &V_a(z,\omega,\omega'') = V_b(\omega,\omega'',z) = 0 \end{aligned} \tag{66}$$

As in the frequency conversion case they can be solved via an iterative approach. Details of this calculation and the numerical errors in the solution method are give in Appendix F. The program code is available, together with the frequency conversion code, on our website.

## 16. PDC: Comparison between simplified analytical and rigorous approach

In sections 14 and 15 we presented two models describing parametric down-conversion: a simple analytic model excluding time-ordering effects and a complex numerical model including time-ordering. As in the frequency conversion case the analytic method is straightforward and only requires minimal computational effort while the rigorous approach demands the solution of coupled integro-differential equations. In this section we compare these two approaches in order to test the validity of our simplified theory for the modelling of parametric down-conversion and the effects of time-ordering present in the rigorous approach.

As in the frequency conversion case, presented in section 8, we consider a correlated and an almost uncorrelated process pumped by ultrafast pump lasers (see Appendix E for the process properties and Appendix F for details on the numerical implementation).

The crucial parameters in the solution are the $\left|V_{a/b}(\omega,\omega')\right|$ amplitudes in the general solution in (51) which describe the amount of EPR-squeezing that is generated during the nonlinear interaction.

The resulting $|V_a(\omega,\omega')|$ for a correlated parametric down-conversion process is depicted in figure 8. The results for uncorrelated parametric down-conversion are visualized in figure 9. Similar to the frequency conversion case we choose to depict the low down-conversion regime in (a), the regime where first discrepancies occur in (b) and the effects in the high down-conversion regime in (c).

The corresponding EPR squeezing values and mode shapes are depicted in figures 10 and 11 for rising down-conversion rates from (a) to (c). The figures in the column on the left shows the squeezing squeezing values obtained via the relation: $\text{squeezing[dB]} = -10\log_{10}\left(e^{-2r_k}\right)$ and the corresponding mean-photon number of the

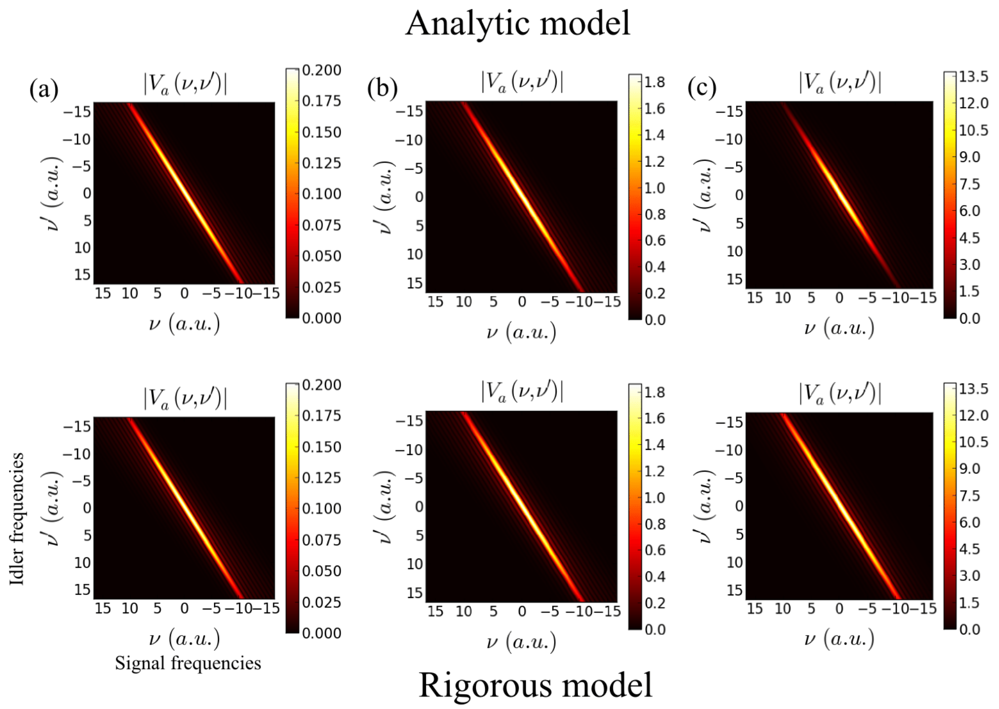

**Figure 8.** Comparison of the process amplitudes $|V_a(\omega,\omega')|$ between the rigorous and the simplified analytical model for a correlated parametric down-conversion process. In the low squeezing regime in (a) both models yield identical results ($\langle n\rangle = 0.59/0.60$ in the analytic / rigours model.). Only at EPR squeezing values of 12 dB, presented in (b), minor discrepancies start to appear ($\langle n\rangle = 44.14/53.18$). Significant differences are only present for extremely high down-conversion rates visualized in (c) ($\langle n\rangle = 1708.16/3328.27$).

complete state, whereas the two columns on the right present the corresponding mode functions $\varphi_1(\nu), \psi_1(\nu), \phi(\nu)$ and $\xi_1(\nu)$ for the first optical mode, where $\varphi_1(\nu)$ and $\psi_1(\nu)$ as well as $\phi_1(\nu)$ and $\xi_1(\nu)$ are of identical shape. "Analytic model" labels the solution excluding time-ordering effects, as presented in section 14 and the "Rigorous model" label marks the rigorous solution from section 15.

Up to squeezing values of 12dB presented in (b) the two approaches give identical results, only when squeezing values beyond this bound are considered significant differences between the two models start to appear. The rigorous model predicts more squeezing than the analytic model and the relaxed energy conservation condition induces a broadening of the spectral distributions $\left|V_{a/b}(\omega,\omega')\right|$ which leads to a broadening of the mode shapes in the high gain regime. In general the impacts of time-ordering on correlated PDC are much weaker than the changes present in the uncorrelated PDC case.

In summary the analytical model accurately describes parametric down-conversion in the low gain regime up to two-mode squeezing values of 12dB, where minor deviations start to appear. Only for extremely high squeezing values, in the range of 20dB and higher, complicated non-trivial deviations from the analytical appear and give significant contribution which require a rigorous treatment of

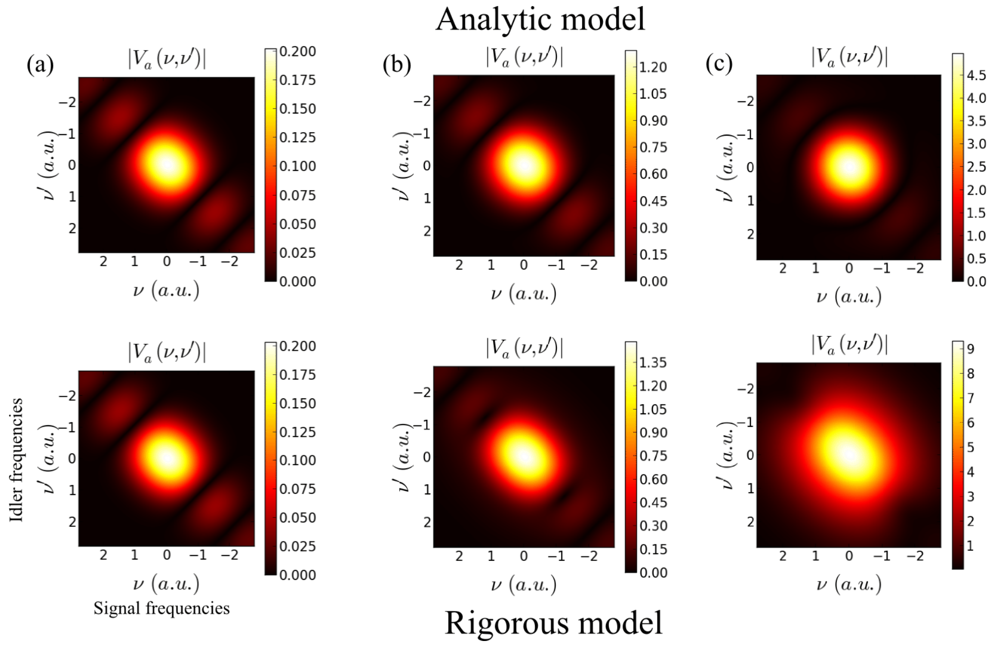

**Figure 9.** Comparison of the process amplitudes $|V_a(\omega, \omega')|$ between the rigorous and the simplified analytical model for an almost uncorrelated parametric down-conversion process. In the low squeezing regime in (a) both models yield identical results ($\langle n \rangle$ = 0.07/0.07 in the analytic / rigours model.). Only at EPR squeezing values of 12 dB, presented in (b), minor discrepancies start to appear ($\langle n \rangle$ = 2.80/4.08). Significant differences are only present for extremely high down-conversion rates visualized in (c) ($\langle n \rangle$ = 39.39/279.87).

parametric down-conversion. For most experimental setups and applications it is hence perfectly justified to apply the simplified analytic model to minimize the computational effort, as long as its limitations are kept in mind.

## 17. PDC: Outlook

The time-ordering effects on PDC have practical implementations for the deployment of PDC sources in quantum optical experiments. In contrast to FC, however, the time-ordering effects are beneficial to the performance of the sources. They lead to much higher EPR squeezing values as predicted by the simplified analytic model.

## 18. Conclusion

In conclusion we developed two models for the nonlinear optical processes of frequency conversion and parametric down-conversion taking into account higher-order photon number effects. The presented rigorous numerical model relies on the solution of coupled differential equations, whereas ignoring time-ordering effects enabled us to construct an analytical solution.

Our analysis revealed that the analytic model gives accurate results for frequency conversion processes up to unit conversion efficiency and parametric down-conversion

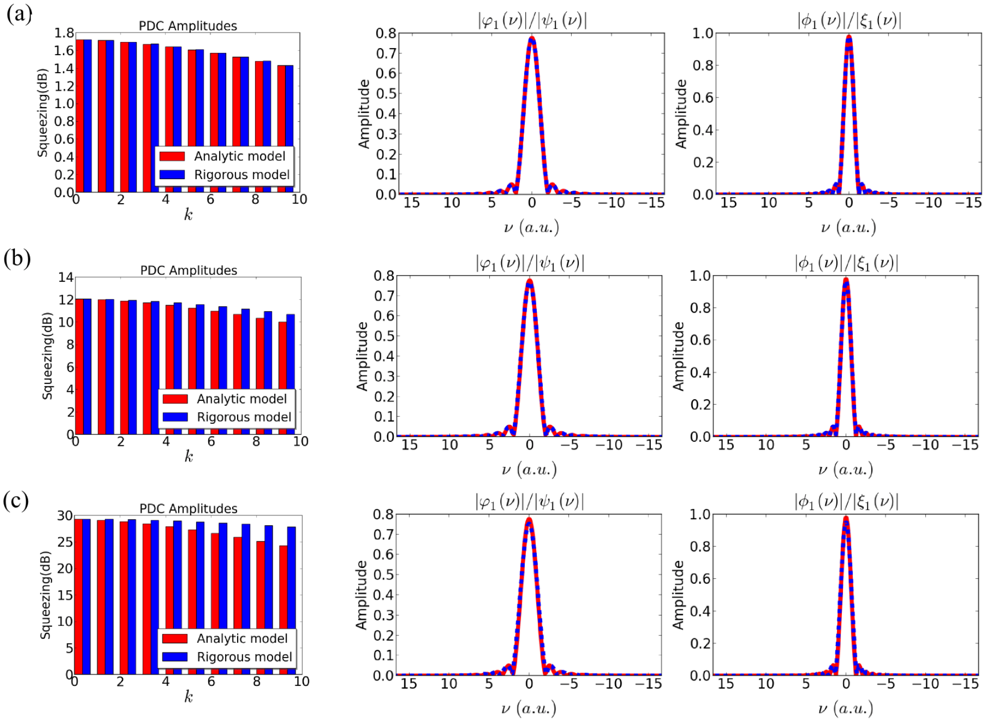

**Figure 10.** Comparison between the rigorous and the analytical approach in correlated many mode parametric down-conversion. For low down-conversion rates, presented in (a), both approaches evaluate to identical results. Only in the case of rising squeezing values in (b), with squeezing values about 12dB, the two approaches start to show minor differences, which become more prominent when even higher squeezing values are considered (c).

process up to 12dB of squeezing. However as soon as we go beyond these bounds, the relaxed energy conservation conditions, induced by the time-ordering effects, require a rigorous treatment of these processes.

The developed fundamental understanding of frequency conversion and parametric down-conversion gives valuable insights into the quantum properties of the nonlinear optical processes, extends the current theoretical descriptions of FC and PDC, and simplifies considerably the engineering process for future quantum information applications.

## 19. Acknowledgments

The authors thank Agata M. Brańczyk and Regina Kruse for useful discussions and helpful comments.

The research leading to these results has received funding from the European Community's Seventh Framework Programme FP7/2007-2013 under the grant agreement Q-Essence 248095.

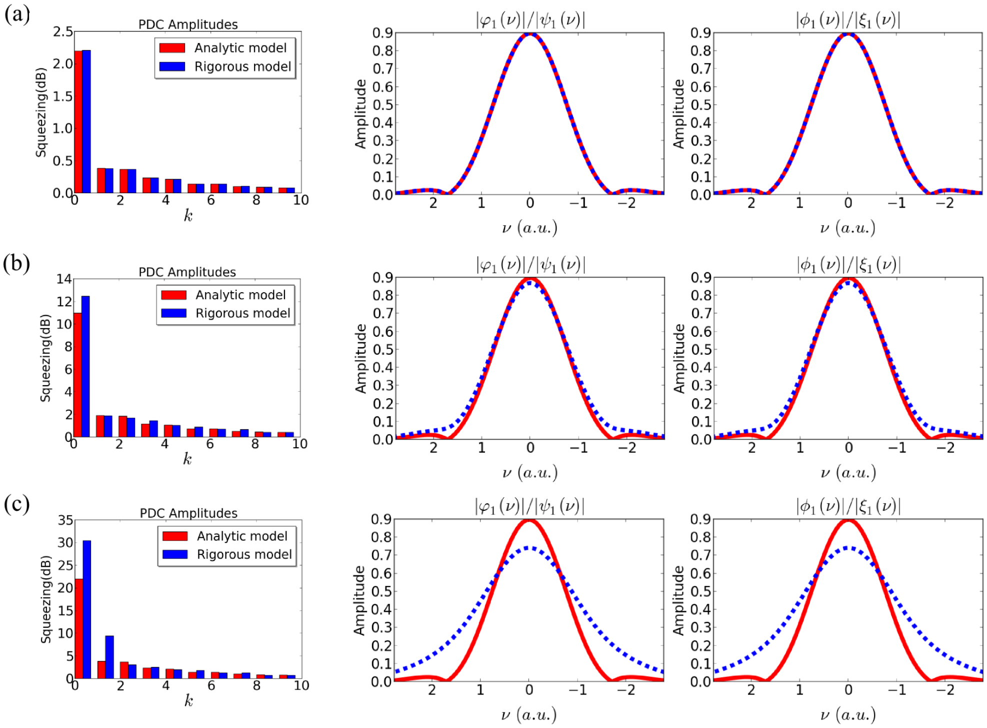

**Figure 11.** Comparison between the rigorous and the analytical approach in (almost) uncorrelated few mode parametric down-conversion. For low down-conversion rates, presented in (a), both approaches evaluate to identical results. Only in the case of rising squeezing values in (b), with squeezing values about 12dB, the two approaches start to show minor differences, which become more prominent when even higher squeezing values are considered (c).

## Appendix A. FC: Canonical transformation conditions

The frequency conversion process in (10) is a unitary transformation, hence the generated output modes must preserve the canonical commutation relations. This imposes several restrictions on the structure of the solution. We evaluate these by extending the calculations from [38, 39] to frequency conversion. At first we rewrite (10) in the more compact notation

$$\begin{aligned} \hat{a}_i^{(out)} &= u_{ij}^{(a)}\hat{a}_j^{(in)} + v_{ij}^{(a)}\hat{c}_j^{(in)} \\ \hat{c}_i^{(out)} &= u_{ij}^{(c)}\hat{c}_j^{(in)} - v_{ij}^{(c)}\hat{a}_j^{(in)} \end{aligned} \tag{A.1}$$

where $i$ and $j$ label the individual frequencies of the electric fields and summation over repeated indices is understood. These two input-output relations must preserve:

$$\begin{aligned} &\left[\hat{a}_i, \hat{a}_j^\dagger\right] = \left[\hat{c}_i, \hat{c}_j^\dagger\right] = \delta_{ij} \\ &\left[\hat{a}_i, \hat{c}_j^\dagger\right] = 0 \end{aligned} \tag{A.2}$$

Using (A.1) and (A.2) we obtain three conditions for frequency conversion:

$$U_a U_a^\dagger + V_a V_a^\dagger \ = U_c U_c^\dagger + V_c V_c^\dagger \ = \mathbb{1} \tag{A.3}$$

$$U_a V_c^\dagger - V_a U_c^\dagger \;=\; 0 \tag{A.4}$$

Furthermore the commutation relations have to be preserved for the inverse transformation as well:

$$\begin{aligned}\hat{a}_i^{(in)} &= u_{ji}^{*(a)} \hat{a}_j^{(out)} - v_{ji}^{*(c)} \hat{c}_j^{(out)} \\ \hat{c}_i^{(in)} &= u_{ji}^{*(c)} \hat{c}_j^{(out)} + v_{ji}^{*(a)} \hat{a}_j^{(out)}.\end{aligned} \tag{A.5}$$

With (A.5) the canonical commutation conditions in (A.2) yield the restrictions:

$$U_a^\dagger U_a + V_c^\dagger V_c \;=\; U_c^\dagger U_c + V_a^\dagger V_a \;=\; \mathbb{1} \tag{A.6}$$

$$U_a^\dagger V_a - V_c^\dagger U_c \;=\; 0 \tag{A.7}$$

The equations (A.3), (A.4), (A.6) and (A.7) impose several constraints on the solution. However they are rather unintuitive representations of the symmetries governing the frequency conversion process, yet with the help of the Bloch-Messiah reduction [39] it is possible to unravel their underlying structure: As a first step we decompose the four matrices $U_a, V_a, U_c, V_c$ as

$$\begin{aligned}U_a &= A_a^u D_a^u B_a^{u\dagger} \qquad & V_a &= A_a^v D_a^v B_a^{v\dagger} \\ U_c &= A_c^u D_c^u B_c^{u\dagger} \qquad & V_c &= A_c^v D_c^v B_c^{v\dagger}\end{aligned} \tag{A.8}$$

where $A$ and $B$ are unitary matrices and $D$ is a diagonal matrix with real entries. This definition is equivalent to a singular-value decomposition except for the fact that we allow the individual elements in $D$ to exhibit negative values.*

The matrices $U_a U_a^\dagger$ and $V_a V_a^\dagger$ are Hermitian and (A.3) implies that they commute hence both are diagonalised by the same unitary matrix $P$:

$$P\, U_a U_a^\dagger P^\dagger = D \qquad P\, V_a V_a^\dagger P^\dagger = D' \tag{A.9}$$

With the help of the decomposition in (A.8) they take on the form:

$$P A_a^u D_a^{u^2} A_a^{u^\dagger} P^\dagger = D \qquad P A_a^v D_a^{v^2} A_a^{v^\dagger} P^\dagger = D' \tag{A.10}$$

And we obtain $A_a^u = A_a^v$. From (A.3) using $U_c U_c^\dagger$ and $V_c V_c^\dagger$ we infer in a similar manner $A_c^u = A_c^v$. Evaluating the conditions for the inverse transformation using (A.6) yields $B_a^u = B_c^v$ and $B_c^u = B_a^v$. Consequently the decomposition in (A.8) can be written as:

$$\begin{aligned}U_a &= A_a D_a^u B_a^\dagger \qquad & U_c &= A_c D_c^u B_c^\dagger \\ V_a &= A_a D_a^v B_c^\dagger \qquad & V_c &= A_c D_c^v B_a^\dagger\end{aligned} \tag{A.11}$$

Using the matrices in (A.11) in conjunction with the conditions in (A.3) we further obtain:

$$D_a^{u^2} + D_a^{v^2} = \mathbb{1} \qquad D_c^{u^2} + D_c^{v^2} = \mathbb{1}. \tag{A.12}$$

This implies that the individual elements of the $D$ matrices have to obey $\cos(r_k)$ and $\sin(r_k)$ behaviour. Applying the conditions in (A.6) to the transformation matrices in (A.11) results in:

$$D_a^{u2} + D_c^{v2} = \mathbb{1} \qquad D_c^{u2} + D_a^{v2} = \mathbb{1} \tag{A.13}$$

From which we conclude $D_a^{u^2} = D_c^{u^2} = D^{u^2}$ and $D_a^{v^2} = D_c^{v^2} = D^{v^2}$. Taking everything into account the final decomposed frequency conversion matrices read:

$$\begin{aligned}U_a &= A_a D^u B_a^\dagger \qquad & U_c &= A_c D^u B_c^\dagger \\ V_a &= A_a D^v B_c^\dagger \qquad & V_c &= A_c D^v B_a^\dagger \\ & & D^{u^2} + D^{v^2} &= \mathbb{1}\end{aligned} \tag{A.14}$$

---

* The reason for this extension of the singular-value decomposition becomes clear in (A.16).

In the original representation they take on the form:

$$\begin{aligned}
U_a(\omega,\omega') &= \sum_k \varphi_k^*(\omega)\cos(r_k)\psi_k(\omega') \\
V_a(\omega,\omega') &= \sum_k \varphi_k^*(\omega)\sin(r_k)\phi_k(\omega') \\
U_c(\omega,\omega') &= \sum_k \xi_k^*(\omega)\cos(r_k)\phi_k(\omega') \\
V_c(\omega,\omega') &= \sum_k \xi_k^*(\omega)\sin(r_k)\psi_k(\omega') \qquad \text{(A.15)}
\end{aligned}$$

From these symmetry relations the frequency conversion process in (10) must take on the form of multiple beam-splitter relations in orthogonal modes

$$\begin{aligned}
\hat{A}_k^{(out)} &= \cos(r_k)\hat{A}_k^{(in)} + \sin(r_k)\hat{C}_k^{(in)} \\
\hat{C}_k^{(out)} &= \cos(r_k)\hat{C}_k^{(in)} - \sin(r_k)\hat{A}_k^{(in)} \qquad \text{(A.16)}
\end{aligned}$$

where we defined:

$$\begin{aligned}
\hat{A}_k^{(out)} &= \int \mathrm{d}\omega\, \varphi_k(\omega)\hat{a}^{(out)}(\omega) \qquad & \hat{C}_k^{(out)} &= \int \mathrm{d}\omega\, \xi_k(\omega)\hat{c}^{(out)}(\omega) \\
\hat{A}_k^{(in)} &= \int \mathrm{d}\omega\, \psi_k(\omega)\hat{a}^{(in)}(\omega) \qquad & \hat{C}_k^{(in)} &= \int \mathrm{d}\omega\, \phi_k(\omega)\hat{c}^{(in)}(\omega) \qquad \text{(A.17)}
\end{aligned}$$

Note however that the canonical commutation relations do not demand that the input and output modes are of identical shape. In principle the input modes $\hat{A}^{(in)}$ and output modes $\hat{C}^{(in)}$ could feature completely different spectral mode functions $\varphi_k(\omega)$ and $\psi_k(\omega)$ but still form a canonical and hence unitary solution.

## Appendix B. PDC: Canonical transformation conditions

As in the case of frequency conversion the parametric down-conversion process is a unitary transformation, hence it must preserve the canonical commutation relations. Retracting the calculation in (Appendix A) for parametric down-conversion they read:

$$U_a U_a^\dagger - V_a V_a^\dagger \;=\; U_b U_b^\dagger - V_b V_b^\dagger \;=\; I \qquad \text{(B.1)}$$

$$U_a V_b^T - V_a U_b^T \;=\; 0 \qquad \text{(B.2)}$$

For the inverse transformation they evaluate to:

$$U_a^\dagger U_a - (V_b^\dagger V_b)^T \;=\; U_b^\dagger U_b - (V_a^\dagger V_a)^T \;=\; I \qquad \text{(B.3)}$$

$$U_a^\dagger V_a - (U_b^\dagger V_b)^T \;=\; 0 \qquad \text{(B.4)}$$

With the help of the singular-value-decomposition theorem and (B.1), (B.2) and (B.4) the four matrices of a general parametric down-conversion process in (51) take on the form:

$$\begin{aligned}
U_a(\omega,\omega') &= \sum_k \varphi_k^*(\omega)\cosh(r_k)\psi_k(\omega') \\
V_a(\omega,\omega') &= \sum_k \varphi_k^*(\omega)\sinh(r_k)\phi_k^*(\omega') \\
U_b(\omega,\omega') &= \sum_k \xi_k^*(\omega)\cosh(r_k)\phi_k(\omega') \\
V_b(\omega,\omega') &= \sum_k \xi_k^*(\omega)\sinh(r_k)\psi_k^*(\omega') \qquad \text{(B.5)}
\end{aligned}$$

From these symmetry relations the parametric down-process (51) consists of multiple twin-beam squeezers in orthogonal optical modes:♯

$$\begin{aligned}\hat{A}_k^{(out)} &= \cosh(r_k)\hat{A}_k^{(in)} + \sinh(r_k)\hat{B}_k^{(in)\dagger}\\ \hat{B}_k^{(out)} &= \cosh(r_k)\hat{B}_k^{(in)} + \sinh(r_k)\hat{A}_k^{(in)\dagger}\end{aligned} \tag{B.6}$$

where we defined:

$$\begin{aligned}\hat{A}_k^{(out)} &= \int \mathrm{d}\omega\, \varphi_k(\omega)\hat{a}^{(out)}(\omega) \qquad & \hat{B}_k^{(out)} &= \int \mathrm{d}\omega\, \xi_k(\omega)\hat{b}^{(out)}(\omega)\\ \hat{A}_k^{(in)} &= \int \mathrm{d}\omega\, \psi_k(\omega)\hat{a}^{(in)}(\omega) \qquad & \hat{B}_k^{(in)} &= \int \mathrm{d}\omega\, \phi_k(\omega)\hat{b}^{(in)}(\omega)\end{aligned} \tag{B.7}$$

Note however that, as in the frequency conversion case, the canonical commutation relations do not demand that the input and output modes are of identical shape.

## Appendix C. FC: Simulated frequency conversion processes

In our simulation of frequency conversion we did not restrict ourselves to a specific crystal material or wavelength range, but created a generic model of the process. For this purpose we first moved from the $(\omega, \omega')$-system to the parameter range $(\nu, \nu')$ relative to the central frequencies of the frequency conversion process $(\omega_0, \omega_0')$. In the simulation we work with a Gaussian pump distribution, as created by pulsed laser systems. The pump distribution in (22) and (41) takes on the form

$$\alpha(\nu - \nu') = E_p \exp\left[-\frac{(\nu - \nu')^2}{2\sigma^2}\right], \tag{C.1}$$

where $E_p$ labels the pump amplitude and $\sigma$ the pump width. The second function we have to adapt is the phasematching function $\Delta k(\omega, \omega') = k_p(\omega' - \omega) - k_c(\omega') + k_a(\omega)$. As a first step we perform a Taylor expansion of the individual $k(\omega)$ terms up to first order about their central frequency $\omega_0$:

$$k(\omega) \approx k(\omega_0) + \frac{d}{d\omega}k(\omega_0)\underbrace{(\omega - \omega_0)}_{\nu} \tag{C.2}$$

This is justified since we restrict ourselves to nonlinear processes not to broad in frequency (slowly varying envelope approximation $\Delta\omega \ll \omega_0$) far off any singularities in the dispersion relation. At the central frequencies the process, per definition, displays perfect phasematching $k_p(\omega_0' - \omega_0) - k_c(\omega_0') + k_a(\omega_0) = 0$ and the phasematching function simplifies to:

$$\Delta k(\nu, \nu') = \frac{d}{d\omega}k_p(\omega_0' - \omega_0)(\nu' - \nu) - \frac{d}{d\omega}k_c(\omega_0')\,\nu' + \frac{d}{d\omega}k_a(\omega_0)\,\nu \tag{C.3}$$

The three remaining parameters $\frac{d}{d\omega}k_p(\omega_0' - \omega_0)$, $\frac{d}{d\omega}k_c(\omega_0')$ and $\frac{d}{d\omega}k_a(\omega_0)$ — the inverse group velocities of the three interacting beams — define the material properties of the system and can be adjusted accordingly.

This compact notation enables us to simulate any frequency conversion process with the help of just 6 parameters: The width and amplitude of the pump beam, the group velocities of the three interacting waves and the length of the nonlinear medium.

---

♯ In principle the twin-beam squeezer has a phase degree of freedom [11] which we absorb in the definition of the electric field operators $\hat{A}_k$ and $\hat{B}_k$.

In order to evaluate a correlated FC with many modes $r_k$, as presented in figure 3 and 5, we use the parameters $\sigma = 4.0$, $\frac{d}{d\omega}k_p(\omega_0' - \omega_0) = 0.5$, $\frac{d}{d\omega}k_c(\omega_0') = 3.0$, $\frac{d}{d\omega}k_a(\omega_0) = 4.5$ and a crystal of length $L = 2$. The pump amplitude $E_p$ is adjusted to give the targeted down-conversion rates.

For the (almost) uncorrelated case with few optical modes $r_k$, as depicted in figure 4 and 6, we applied $\sigma = 0.98190$, $\frac{d}{d\omega}k_p(\omega_0' - \omega_0) = 3.0$, $\frac{d}{d\omega}k_c(\omega_0') = 1.5$, $\frac{d}{d\omega}k_a(\omega_0) = 4.5$ and a crystal of length $L = 2$. Again the pump amplitude $E_p$ is adjusted to give the desired down-conversion rates.

## Appendix D. FC: Numerical implementation

In order to obtain the time-ordered solutions we solved the classical differential equations in (44) and (45) which give the functions $U_a(z,\omega,\omega'')$, $U_c(z,\omega,\omega'')$, $V_a(z,\omega,\omega'')$, and $V_c(z,\omega,\omega'')$ describing the frequency conversion process.

In the numerical implementation of frequency conversion we used a sampling of 500 points for each frequency degree of freedom and 500 points in $z$-direction to discretize the functions $U_a(z,\omega,\omega'')$, $U_c(z,\omega,\omega'')$, $V_a(z,\omega,\omega'')$, $V_c(z,\omega,\omega'')$ and $f(\omega,\omega',z)$. We evaluated the successive integrations in (46) via the trapezoid rule until the solutions converged. The actual solution defining the overall process properties is given by the matrices at the end of the crystal $U_a(z = \frac{L}{2},\omega,\omega'')$, $U_c(z = \frac{L}{2},\omega,\omega'')$, $V_a(z = \frac{L}{2},\omega,\omega'')$, and $V_c(z = \frac{L}{2},\omega,\omega'')$

We checked the accuracy of the result in a variety of ways: At first we evaluated the canonical transformation conditions in (A.3), (A.4), (A.6), and (A.7). For example in the case of (A.4) we calculated:

$$\begin{aligned}
&\int \mathrm{d}\omega' U_a(z = \frac{L}{2},\omega,\omega')V_c(z = \frac{L}{2},\omega'',\omega')^* \\
&\qquad - \int \mathrm{d}\omega' V_a(z = \frac{L}{2},\omega,\omega')U_c(z = \frac{L}{2},\omega'',\omega')^* \\
&\qquad = D^{(diff)}(z = \frac{L}{2},\omega,\omega')
\end{aligned} \tag{D.1}$$

and determined the distance of $D^{(diff)}(z = \frac{L}{2},\omega,\omega')$ from the expected zero matrix and consequently the error in the solution via:

$$\text{error} = \frac{\int \mathrm{d}\omega \int \mathrm{d}\omega' D^{(diff)}(z = \frac{L}{2},\omega,\omega')}{0.5\left[\int \mathrm{d}\omega \int \mathrm{d}\omega' |V_a(z = \frac{L}{2},\omega,\omega')| + \int \mathrm{d}\omega \int \mathrm{d}\omega' |U_c(z = \frac{L}{2},\omega,\omega')|\right]} \tag{D.2}$$

In all presented cases the obtained error was below 0.0085.

We also checked the numerical Schmidt decompositions of $U_a(z = \frac{L}{2},\omega,\omega'')$, $U_c(z = \frac{L}{2},\omega,\omega'')$, $V_a(z = \frac{L}{2},\omega,\omega'')$, and $V_c(z = \frac{L}{2},\omega,\omega'')$ to verify the mode properties derived in Appendix A. During this process the decompositions of $U_a(z = \frac{L}{2},\omega,\omega'')$, $U_c(z = \frac{L}{2},\omega,\omega'')$ showed numerical issues, these however could be resolved by decomposing $U_a(z = \frac{L}{2},\omega,\omega'')U_a^\dagger(z = \frac{L}{2},\omega,\omega'')$, $U_a^\dagger(z = \frac{L}{2},\omega,\omega'')U_a(z = \frac{L}{2},\omega,\omega'')$, $U_c(z = \frac{L}{2},\omega,\omega'')U_c^\dagger(z = \frac{L}{2},\omega,\omega'')$, $U_c^\dagger(z = \frac{L}{2},\omega,\omega'')U_c(z = \frac{L}{2},\omega,\omega'')$ instead. The obtained modes from these four matrices provided a much improved stability especially in the high gain regime. Using these Schmidt modes we verified that the obtained Schmidt values of the $U$ and $V$ matrices behaved like $\cos(r_k)^2 + \sin(r_k)^2 = 1$ with errors below 0.0063. We also asserted that the decompositions yielded the functions $\varphi_k, \psi_k, \phi_k, \xi_k$ with symmetries as detailed in (A.15), which were fulfilled within numerical accuracy.

The program code, published on our website, is able to directly create the investigated frequency conversion processes and also performs all mentioned tests.

## Appendix E. PDC: Simulated down-conversion process

As in the simulation of frequency conversion processes in Appendix C we didn't restrict ourselves to a specific crystal material and wavelength range but created a generic model of the process. Again we first move from the $(\omega, \omega')$-system to the parameter range $(\nu, \nu')$ relative to the central frequencies of the parametric down-conversion process $(\omega_0, \omega_0')$. As in the frequency conversion case we used a Gaussian pump distribution for the simulation, which in (56) and (61) take on the form

$$\alpha(\nu + \nu') = E_p \exp\left[-\frac{(\nu + \nu')^2}{2\sigma^2}\right], \tag{E.1}$$

where $E_p$ labels the pump amplitude and $\sigma$ the pump width. The second function we have to adapt is the phase-matching function $\Delta k(\omega, \omega') = k_p(\omega + \omega') - k_a(\omega) - k_b(\omega')$. As a first step we perform a Taylor expansion of the individual $k(\omega)$ terms up to first order about their central frequency $\omega_0$:

$$k(\omega) \approx k(\omega_0) + \frac{d}{d\omega} k(\omega_0) \underbrace{(\omega - \omega_0)}_{\nu} \tag{E.2}$$

This is justified since we restrict ourselves to nonlinear processes not to broad in frequency (slowly varying envelope approximation $\Delta\omega \ll \omega_0$) far off any singularities in the dispersion. At the central frequencies the process, per definition, displays perfect phasematching $k_p(\omega_0' + \omega_0) - k_a(\omega_0) - k_b(\omega_0') = 0$ and the phasematching function simplifies to:

$$\Delta k(\nu, \nu') = \frac{d}{d\omega} k_p(\omega_0' + \omega_0)(\nu' + \nu) - \frac{d}{d\omega} k_a(\omega_0)\, \nu - \frac{d}{d\omega} k_b(\omega_0')\, \nu' \tag{E.3}$$

The three remaining parameters $\frac{d}{d\omega} k_p(\omega_0' + \omega_0)$, $\frac{d}{d\omega} k_a(\omega_0)$ and $\frac{d}{d\omega} k_b(\omega_0')$ — the inverse group velocities of the three interacting beams — define the material properties of the system and can be adjusted accordingly.

This compact notation enables us to simulate any parametric down-conversion conversion process with the help of just 6 parameters: The width and amplitude of the pump beam, the group velocities of the three interacting waves and the length of the nonlinear medium.

In order to evaluate a correlated PDC with many modes $r_k$, as presented in figure 8 and 10, we use the parameters $\sigma = 4.0$, $\frac{d}{d\omega} k_p(\omega_0' + \omega_0) = 0.5$, $\frac{d}{d\omega} k_a(\omega_0) = 3.0$, $\frac{d}{d\omega} k_b(\omega_0') = 4.5$ and a crystal of length $L = 2$. The pump amplitude $E_p$ is adjusted to give the targeted conversion efficiencies.

For the (almost) uncorrelated case with few optical modes $r_k$, as depicted in figures 9 and 11, we applied $\sigma = 0.96231155$, $\frac{d}{d\omega} k_p(\omega_0 + \omega_0') = 3.0$, $\frac{d}{d\omega} k_a(\omega_0) = 4.5$, $\frac{d}{d\omega} k_b(\omega_0') = 1.5$ and a crystal of length $L = 2$. Again the pump amplitude $E_p$ is adjusted to give the desired conversion efficiencies.

## Appendix F. PDC: Numerical implementation

In order to obtain the time-ordered solutions we solved the classical differential equations in (64) and (65) which give the functions $U_a(z, \omega, \omega'')$, $U_b(z, \omega, \omega'')$, $V_a(z, \omega, \omega'')$, and $V_b(z, \omega, \omega'')$ describing the parametric down-conversion process.

In the numerical implementation of parametric down-conversion we used a sampling of 500 points for each frequency degree of freedom and 500 points in $z$-direction to discretize the functions $U_a(z,\omega,\omega'')$, $U_b(z,\omega,\omega'')$, $V_a(z,\omega,\omega'')$, $V_b(z,\omega,\omega'')$ and $f(\omega,\omega',z)$. As in the frequency conversion case we evaluated the successive integrations via the trapezoid rule until the solutions converged. The actual solution defining the overall process properties is given by the matrices at the end of the crystal $U_a(z=\frac{L}{2},\omega,\omega'')$, $U_b(z=\frac{L}{2},\omega,\omega'')$, $V_a(z=\frac{L}{2},\omega,\omega'')$, and $V_b(z=\frac{L}{2},\omega,\omega'')$

We checked the accuracy of the result in a variety of ways: At first we evaluated the canonical transformation conditions in (B.1), (B.2), (B.3), and (B.4). For example in the case of (B.2) we evaluated:

$$\begin{aligned}\int \mathrm{d}\omega' U_a(z=\frac{L}{2},\omega,\omega')V_b(z=\frac{L}{2},\omega'',\omega')\\ -\int \mathrm{d}\omega' V_a(z=\frac{L}{2},\omega,\omega')U_b(z=\frac{L}{2},\omega'',\omega')\\ = D^{(diff)}(z=\frac{L}{2},\omega,\omega') \qquad \text{(F.1)}\end{aligned}$$

and determined the distance of $D^{(diff)}(z=\frac{L}{2},\omega,\omega')$ from the expected zero matrix and consequently the error in the solution via:

$$\text{error} = \frac{\int \mathrm{d}\omega \int \mathrm{d}\omega' D^{(diff)}(z=\frac{L}{2},\omega,\omega')}{0.5\left[\int \mathrm{d}\omega \int \mathrm{d}\omega' |V_a(z=\frac{L}{2},\omega,\omega')| + \int \mathrm{d}\omega \int \mathrm{d}\omega' |U_b(z=\frac{L}{2},\omega,\omega')|\right]} \qquad \text{(F.2)}$$

In all presented cases the obtained error was below 0.00019.

We also checked the numerical Schmidt decompositions of $U_a(z,\omega,\omega'')$, $U_b(z,\omega,\omega'')$, $V_a(z,\omega,\omega'')$, and $V_b(z,\omega,\omega'')$ to verify the mode properties derived in Appendix B. During this process the decompositions of $U_a(z,\omega,\omega'')$, $U_b(z,\omega,\omega'')$ showed numerical issues, these however could be resolved by decomposing $U_a(z,\omega,\omega'')U_a^\dagger(z,\omega,\omega'')$, $U_a^\dagger(z,\omega,\omega'')U_a(z,\omega,\omega'')$, $U_b(z,\omega,\omega'')U_b^\dagger(z,\omega,\omega'')$, $U_b^\dagger(z,\omega,\omega'')U_b(z,\omega,\omega'')$ instead. The obtained modes from these four matrices provided a much improved stability especially in the high gain regime. Using these Schmidt modes we verified that the obtained Schmidt values of the $U$ and $V$ matrices behaved like $\cosh(r_k)^2 - \sinh(r_k)^2 = 1$ with errors below 0.00006. We also asserted that the decompositions yielded the functions $\varphi_k, \psi_k, \phi_k, \xi_k$ with symmetries as detailed in (B.5), which where fulfilled within numerical accuracy.

The program code, published on our website, is able to directly create the investigated parametric down-conversion processes and also performs all mentioned tests.

## References

[1] C. K. Hong, Z. Y. Ou, and L. Mandel. Measurement of subpicosecond time intervals between two photons by interference. *Physical Review Letters*, 59(18):2044, November 1987.

[2] Alfred B. U'Ren, Christine Silberhorn, Konrad Banaszek, and Ian A. Walmsley. Efficient conditional preparation of high-fidelity single photon states for fiber-optic quantum networks. *Physical Review Letters*, 93(9):093601, 2004.

[3] Peter J. Mosley, Jeff S. Lundeen, Brian J. Smith, Piotr Wasylczyk, Alfred B. U'Ren, Christine Silberhorn, and Ian A. Walmsley. Heralded generation of ultrafast single photons in pure quantum states. *Physical Review Letters*, 100(13):133601–4, April 2008.

[4] T.B. Pittman, B.C. Jacobs, and J.D. Franson. Heralding single photons from pulsed parametric down-conversion. *Optics Communications*, 246(4-6):545–550, February 2005.

[5] A. L. Migdall, D. Branning, and S. Castelletto. Tailoring single-photon and multiphoton probabilities of a single-photon on-demand source. *Physical Review A*, 66(5):053805, November 2002.

[6] Paul G. Kwiat, Klaus Mattle, Harald Weinfurter, Anton Zeilinger, Alexander V. Sergienko, and Yanhua Shih. New high-intensity source of polarization-entangled photon pairs. *Physical Review Letters*, 75(24):4337–4341, December 1995.

[7] Paul G. Kwiat, Edo Waks, Andrew G. White, Ian Appelbaum, and Philippe H. Eberhard. Ultrabright source of polarization-entangled photons. *Physical Review A*, 60(2):R773–R776, 1999.

[8] Christian Kurtsiefer, Markus Oberparleiter, and Harald Weinfurter. High-efficiency entangled photon pair collection in type-II parametric fluorescence. *Physical Review A*, 64(2):023802, July 2001.

[9] Matthew E. Anderson, D. F. McAlister, M. G. Raymer, and Mool C. Gupta. Pulsed squeezed-light generation in chiˆ(2) nonlinear waveguides. *Journal of the Optical Society of America B*, 14(11):3180, November 1997.

[10] D. K. Serkland, M. M. Fejer, R. L. Byer, and Y. Yamamoto. Squeezing in a quasi-phase-matched LiNbO3 waveguide. *Optics Letters*, 20(15):1649–1651, 1995.

[11] Stephen M. Barnett and Paul M. Radmore. *Methods in theoretical quantum optics*. Oxford University Press, January 2003.

[12] Andreas Christ, Kaisa Laiho, Andreas Eckstein, Katiúscia N Cassemiro, and Christine Silberhorn. Probing multimode squeezing with correlation functions. *New Journal of Physics*, 13:033027, March 2011.

[13] Xiaorong Gu, Kun Huang, Haifeng Pan, E Wu, and Heping Zeng. Photon correlation in single-photon frequency upconversion. *Optics Express*, 20(3):2399–2407, January 2012.

[14] H. J. McGuinness, M. G. Raymer, C. J. McKinstrie, and S. Radic. Quantum frequency translation of single-photon states in a photonic crystal fiber. *Physical Review Letters*, 105(9):093604, 2010.

[15] L. Mejling, C. J. McKinstrie, M. G. Raymer, and K. Rottwitt. Quantum frequency translation by four-wave mixing in a fiber: low-conversion regime. *Optics Express*, 20(8):8367–8396, April 2012.

[16] S. Tanzilli, W. Tittel, M. Halder, O. Alibart, P. Baldi, N. Gisin, and H. Zbinden. A photonic quantum information interface. *Nature*, 437(7055):116–120, September 2005.

[17] D. Kielpinski, J. F. Corney, and H. M. Wiseman. Quantum optical waveform conversion. *Physical Review Letters*, 106(13):130501, March 2011.

[18] Benjamin Brecht, Andreas Eckstein, Andreas Christ, Hubertus Suche, and Christine Silberhorn. From quantum pulse gate to quantum pulse shaper—engineered frequency conversion in nonlinear optical waveguides. *New Journal of Physics*, 13(6):065029, June 2011.

[19] Andreas Eckstein, Benjamin Brecht, and Christine Silberhorn. A quantum pulse gate based on spectrally engineered sum frequency generation. *Optics Express*, 19(15):13770–13778, July 2011.

[20] H. J. McGuinness, M. G. Raymer, and C. J. McKinstrie. Theory of quantum frequency translation of light in optical fiber: application to interference of two photons of different color. *Optics Express*, 19(19):17876–17907, 2011.

[21] H. Kamada, M. Asobe, T. Honjo, H. Takesue, Y. Tokura, Y. Nishida, O. Tadanaga, and H. Miyazawa. Efficient and low-noise single-photon detection in 1550 nm communication band by frequency upconversion in periodically poled LiNbO3 waveguides. *Optics Letters*, 33(7):639–641, April 2008.

[22] J. S. Pelc, L. Ma, C. R. Phillips, Q. Zhang, C. Langrock, O. Slattery, X. Tang, and M. M. Fejer. Long-wavelength-pumped upconversion single-photon detector at 1550 nm: performance and noise analysis. *Optics Express*, 19(22):21445–21456, October 2011.

[23] J. S. Pelc, Q. Zhang, C. R. Phillips, L. Yu, Y. Yamamoto, and M. M. Fejer. Cascaded frequency upconversion for high-speed single-photon detection at 1550 nm. *Optics Letters*, 37(4):476–478, February 2012.

[24] R. Clark, Taehyun Kim, and Jungsang Kim. Double-stage frequency down-conversion system for distribution of ion-photon entanglement over long distances. In *Photonics Society Summer Topical Meeting Series, 2011 IEEE*, pages 45 –46, July 2011.

[25] S. Ramelow, A. Fedrizzi, A. Poppe, N. K. Langford, and A. Zeilinger. Polarization-entanglement-conserving frequency conversion of photons. *Physical Review A*, 85(1):013845, January 2012.

[26] W. P. Grice and I. A. Walmsley. Spectral information and distinguishability in type-II down-conversion with a broadband pump. *Physical Review A*, 56(2):1627, 1997. Copyright (C) 2009 The American Physical Society; Please report any problems to prola@aps.org.

[27] Wojciech Wasilewski, A. I. Lvovsky, Konrad Banaszek, and Czeslaw Radzewicz. Pulsed squeezed light: Simultaneous squeezing of multiple modes. *Physical Review A (Atomic, Molecular, and Optical Physics)*, 73(6):063819–12, June 2006.

[28] A. I. Lvovsky, Wojciech Wasilewski, and Konrad Banaszek. Decomposing a pulsed optical parametric amplifier into independent squeezers. *Journal of Modern Optics*, 54(5):721, 2007.

[29] E. Brambilla, A. Gatti, M. Bache, and L. A. Lugiato. Simultaneous near-field and far-field spatial quantum correlations in the high-gain regime of parametric down-conversion. *Physical Review A*, 69(2):023802, February 2004. Copyright (C) 2009 The American Physical Society; Please report any problems to prola@aps.org.

[30] Agata M Brańczyk. *Non-classical States of Light*. PhD thesis, University of Queensland, August 2010.

[31] Gil Porat, Yaron Silberberg, Ady Arie, and Haim Suchowski. Two photon frequency conversion. *Optics Express*, 20(4):3613–3619, February 2012.

[32] Mikhail I. Kolobov. The spatial behavior of nonclassical light. *Reviews of Modern Physics*, 71(5):1539, October 1999.

[33] K. J. Blow, Rodney Loudon, Simon J. D. Phoenix, and T. J. Shepherd. Continuum fields in quantum optics. *Physical Review A*, 42(7):4102, October 1990.

[34] Rodney Loudon. *The Quantum Theory of Light*. Oxford University Press, USA, 3 edition, November 2000.

[35] Prem Kumar. Quantum frequency conversion. *Optics Letters*, 15(24):1476–1478, December 1990.

[36] Kevin A. O'Donnell and Alfred B. U'Ren. Time-resolved up-conversion of entangled photon pairs. *Physical Review Letters*, 103(12):123602, 2009.

[37] Richard A. Campos, Bahaa E. A. Saleh, and Malvin C. Teich. Quantum-mechanical lossless beam splitter: SU(2) symmetry and photon statistics. *Physical Review A*, 40(3):1371, 1989.

[38] Artur K. Ekert and Peter L. Knight. Relationship between semiclassical and quantum-mechanical input-output theories of optical response. *Physical Review A*, 43(7):3934, April 1991. Copyright (C) 2009 The American Physical Society; Please report any problems to prola@aps.org.

[39] Samuel L. Braunstein. Squeezing as an irreducible resource. *Physical Review A*, 71(5):055801, May 2005. Copyright (C) 2009 The American Physical Society; Please report any problems to prola@aps.org.

[40] M.G. Raymer, S.J. van Enk, C.J. McKinstrie, and H.J. McGuinness. Interference of two photons of different color. *Optics Communications*, 283(5):747–752, March 2010.

[41] Peter P Rohde, Wolfgang Mauerer, and Christine Silberhorn. Spectral structure and decompositions of optical states, and their applications. *New Journal of Physics*, 9:91–91, April 2007.

[42] J. J. Sakurai. *Modern Quantum Mechanics*. Prentice Hall, revised edition. edition, August 1993.

[43] Agata M. Brańczyk, Thomas M. Stace, and T. C. Ralph. Time ordering in spontaneous parametric down-conversion. *AIP Conference Proceedings*, 1363(1):335–338, October 2011.

[44] C. K. Law, I. A. Walmsley, and J. H. Eberly. Continuous frequency entanglement: Effective finite hilbert space and entropy control. *Physical Review Letters*, 84(23):5304, June 2000.

[45] A. B U'Ren, K. Banaszek, and I. A Walmsley. Photon engineering for quantum information processing. *Quantum Info. Comput.*, 3(7):480–502, October 2003. ACM ID: 2011567.

[46] Wolfgang Mauerer. *On Colours, Keys, and Correlations: Multimode Parametric Downconversion in the Photon Number Basis*. PhD thesis, Universität Erlangen-Nürnberg, Universitätsstraße. 4, 91054 Erlangen, 2008.

[47] L. Caspani, E. Brambilla, and A. Gatti. Tailoring the spatiotemporal structure of biphoton entanglement in type-i parametric down-conversion. *Physical Review A*, 81(3):033808, March 2010.

[48] Wojciech Wasilewski and M. G. Raymer. Pairwise entanglement and readout of atomic-ensemble and optical wave-packet modes in traveling-wave raman interactions. *Physical Review A*, 73(6):063816, June 2006.

[49] Barak Dayan. Theory of two-photon interactions with broadband down-converted light and entangled photons. *Physical Review A*, 76(4):043813, October 2007.

[50] A. Gatti, R. Zambrini, M. San Miguel, and L. A. Lugiato. Multiphoton multimode polarization entanglement in parametric down-conversion. *Physical Review A*, 68(5):053807, November 2003.

[51] Agata M. Branczyk, Alessandro Fedrizzi, Thomas M. Stace, Tim C. Ralph, and Andrew G. White. Engineered optical nonlinearity for quantum light sources. *Optics Express*, 19(1):55–

65, January 2011.

[52] Andreas Christ. *Theory of waveguided parametric down-conversion: From fundamentals to applications (to be published).* PhD thesis, University of Paderborn, 2012.